

AdaSCALE: Adaptive Scaling for OOD Detection

Sudarshan Regmi¹

Abstract

The ability of the deep learning model to recognize when a sample falls outside its learned distribution is critical for safe and reliable deployment. Recent state-of-the-art out-of-distribution (OOD) detection methods leverage activation shaping to improve the separation between in-distribution (ID) and OOD inputs. These approaches resort to sample-specific scaling but apply a static percentile threshold across all samples regardless of their nature, resulting in suboptimal ID-OOD separability. In this work, we propose **AdaSCALE**, an adaptive scaling procedure that dynamically adjusts the percentile threshold based on a sample’s estimated OODness. This estimation leverages our key observation: OOD samples exhibit significantly more pronounced activation shifts at high-magnitude activations under minor perturbation compared to ID samples. AdaSCALE enables stronger scaling for likely ID samples and weaker scaling for likely OOD samples, yielding highly separable energy scores. Our approach achieves state-of-the-art OOD detection performance, outperforming the latest rival OptFS by **14.94%** in near-OOD and **21.67%** in far-OOD datasets in average FPR@95 metric on the ImageNet-1k benchmark across eight diverse architectures.

1. Introduction

The reliable deployment of deep learning models hinges on their ability to handle unknown inputs, a task commonly known as OOD detection. One critical application is in medical diagnosis, where a model trained on common diseases should be able to flag inputs representing unknown conditions as potential outliers, requiring further review by clinicians. OOD detection primarily involves identifying semantic shifts, with robustness to covariate shifts being a highly desirable characteristic (Yang et al., 2023; Baek et al.,

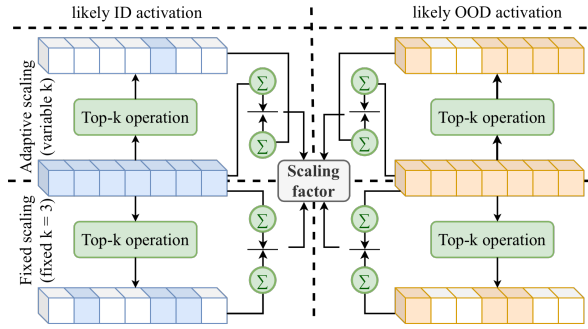


Figure 1. Adaptive scaling (AdaSCALE) vs. fixed scaling (ASH (Djurisic et al., 2023), SCALE (Xu et al., 2024), LTS (Djurisic et al., 2024)). While fixed scaling approaches uses a constant percentile threshold p and hence constant k (e.g., $k = 3$) across all samples, AdaSCALE adjusts k based on estimated OODness. AdaSCALE assigns larger k values (e.g., $k = 5$) to OOD-like samples, yielding smaller scaling factors, and smaller k values (e.g., $k = 1$) to ID-like samples, yielding larger scaling factors. This adaptive mechanism enhances ID-OOD separability. (See Figure 4 for complete working mechanism of AdaSCALE.)

2024). As the modern deep learning models scale in both data and parameter counts, effective OOD detection within the large-scale settings is critical. Given the difficulties of iterating on large models, the *post-hoc* approaches that preserve ID classification accuracy are generally preferred.

A variety of post-hoc approaches have emerged, broadly categorized by where they operate. One class of methods focuses on computing OOD scores directly in the output space (Hendrycks & Gimpel, 2017; Liang et al., 2018; Liu et al., 2020; Hendrycks et al., 2022a; Djurisic et al., 2023; Zhao et al., 2024), while another operates in the activation space (Lee et al., 2018; Sun et al., 2022; Ren et al., 2021; Rajasekaran et al., 2024). Finally, a more recent line of research also explores a hybrid approach (Wang et al., 2022; Kim et al., 2024), combining information from both spaces. The efficacy of many high-performing methods relies on either accurate computation of ID statistics (Sun et al., 2021; Kong & Li, 2022; Xu et al., 2023; Sun & Li, 2022; Krumpl et al., 2024) or retention of training data statistics (Sun et al., 2022; Rajasekaran et al., 2024). However, as retaining full access to training data becomes increasingly impractical in large-scale settings, methods that operate effectively with minimal ID samples are valuable for practical applications.

¹Department of Computer Science, Dartmouth College. Correspondence to: Sudarshan Regmi <sudarshan.regmi.gr@dartmouth.edu>.

Alleviating the dependence on ID training data/statistics, recent state-of-the-art post-hoc approaches center around the concept of “fixed scaling.” ASH (Djurisic et al., 2023) prunes and scales activations on a per-sample basis. SCALE (Xu et al., 2024), the direct successor of ASH, critiques pruning and focuses purely on scaling, which improves OOD detection performance without accuracy degradation. LTS (Djurisic et al., 2024) extends this concept by directly scaling logits instead, using post-ReLu activations. These methods leverage a key insight: scaling based on relative strength of a sample’s *top-k* activations (with respect to entire activations) yields highly separable ID-OOD energy scores. However, although such approaches provide sample-specific scaling factors, the scaling mechanism remains uniform across all samples as the percentile threshold p and thereby k is fixed, as shown in Figure 1. This static approach is inherently limiting for optimal ID-OOD separation while also failing to leverage even minimal ID data, which could be reasonably practical in most scenarios.

We hypothesize that designing an adaptive scaling procedure based on each sample’s estimated OODness offers greater control for enhancing ID-OOD separability. Specifically, this mechanism should assign smaller scaling factors for samples with high OODness to yield lower-magnitude energy scores and larger scaling factors for probable ID samples to yield higher-magnitude energy scores. To achieve this, we propose a heuristic for estimating OODness based on a key observation in activation space: minor perturbations applied to OOD samples induce significantly more pronounced shifts in their top-k activations compared to ID samples. Consequently, samples exhibiting substantial activation shifts are assigned lower scaling factors, while those with minimal shifts receive higher scaling factors. This adaptive scaling mechanism can be applied in either logit or activation space. Our method, AdaSCALE, achieves state-of-the-art performance, delivering significant improvements in OOD detection albeit with higher computational cost while requiring only minimal number of ID samples.

We conduct an extensive evaluation across 8 architectures on ImageNet-1k and 2 architectures on CIFAR benchmarks, demonstrating the substantial effectiveness of AdaSCALE. For instance, AdaSCALE surpasses the average performance of the *best-generalizing* method, OptFS (Zhao et al., 2024), by **14.94% / 8.96%** for near-OOD detection and **21.48% / 3.39%** for far-OOD detection in terms of FPR@95 / AUROC, on the ImageNet-1k benchmark across eight architectures. Furthermore, AdaSCALE outperforms the *best-performing* method, SCALE (Xu et al., 2024), when evaluated on the ResNet-50 architecture, achieving performance gains of **12.95% / 6.44%** for near-OOD and **16.79% / 0.79%** for far-OOD detection. Additionally, AdaSCALE consistently demonstrates superiority in full-spectrum OOD (FSOOD) detection (Yang et al., 2023). Our

key contributions are summarized below:

- We reveal that OOD inputs exhibit more pronounced shifts in top-k activations under minor perturbations compared to ID inputs. Leveraging this, we propose a novel post-hoc OOD detection method using adaptive scaling that attains state-of-the-art OOD detection.
- We demonstrate the state-of-the-art generalization of AdaSCALE via extensive evaluations across 10 architectures and 3 datasets by tuning mere one hyperparameter for a given setup.

2. Related Works

Post-hoc methods. Early research on OOD detection primarily focused on designing scoring functions based on logit information (Hendrycks & Gimpel, 2017; Liang et al., 2018; Liu et al., 2020; Hendrycks et al., 2022a; Liu et al., 2023). While these methods leveraged logit-based scores, alternative approaches have explored gradient-based information, such as GradNorm (Huang et al., 2021), GradOrth (Behpour et al., 2023), GAIA (Chen et al., 2023), and GregOOD (Sharifi et al., 2025). Given the limited dimensionality of the logit space, which may not encapsulate sufficient information for OOD detection, subsequent studies have investigated activation-space-based methods. These approaches exploit the high-dimensional activations, leading to both parametric techniques such as MDS (Lee et al., 2018), MDS Ensemble (Lee et al., 2018), and RMDS (Ren et al., 2021), as well as non-parametric methods such as KNN-based OOD detection (Sun et al., 2022; Park et al., 2023). Recent advancements have proposed hybrid methodologies that integrate parametric and non-parametric techniques to improve robustness. For instance, ComboOOD (Rajasekaran et al., 2024) combines these paradigms to enhance near-OOD detection performance. Similarly, VIM (Wang et al., 2022) employs a combination of logit-based and distance-based metrics. However, reliance of such approaches on ID statistics (Sun & Li, 2022; Olber et al., 2023; Zhang et al., 2023a) can become a constraint, hindering scalability and practical deployment in real-world applications. To mitigate computational challenges for real-world deployment, recent methods, such as FDBD (Liu & Qin, 2024) and NCI (Liu & Qin, 2023), have focused on enhancing efficiency. Recent advances, such as NECO (Ammar et al., 2024) examines connections to neural collapse phenomena, while WeiPer (Granz et al., 2024), explore class-direction perturbations. Unlike WeiPer, our work deals with perturbation in the input similar to ODIN (Liang et al., 2018).

Activation-shaping post-hoc methods. A seminal work in OOD detection, ReAct (Sun et al., 2021), identified abnormally high activation patterns in OOD samples and proposed clipping extreme activations. LINe (Ahn et al.,

2023) integrates activation clipping with Shapley-value-based pruning, selectively masking irrelevant neurons to mitigate noise. Activation clipping has been further generalized by BFAct (Kong & Li, 2022) and VRA (Xu et al., 2023) for enhanced effectiveness. Additionally, BATS (Zhu et al., 2022) refines activation distributions by aligning them with their respective typical sets, while LAPS (He et al., 2024) enhances this strategy by incorporating channel-aware typical sets. Inspired by activation clipping, another line of research explores activation “scaling” as a means to improve OOD detection. ASH (Djurisic et al., 2023) introduces a method to compute a scaling factor as a function of the activation itself, pruning and rescaling activations to enhance the separation of energy scores between ID and OOD samples. However, this approach results in a slight degradation in ID classification accuracy. In response, SCALE (Xu et al., 2024) observes that pruning adversely affects performance and thus eliminates it, leading to improved OOD detection while preserving ID accuracy. SCALE currently represents the state-of-the-art method for ResNet-50-based OOD detection. Despite their efficacy, these activation-based methods exhibit limited generalization across diverse architectures. To address this issue, LTS (Djurisic et al., 2024) extends SCALE by computing scaling factors using post-ReLu activations and applying them directly to logits rather than activations. Our work builds on this line of work, introducing the adaptive scaling mechanism. ATS (Krumpl et al., 2024) argues that relying solely on final-layer activations may result in the loss of critical information beneficial for OOD detection and proposes to leverage intermediate-layer activations too. However, its efficacy is contingent upon the availability of a large number of training samples, whereas our approach attains state-of-the-art performance while utilizing a minimal ID samples. A newly proposed method OptFS (Zhao et al., 2024) introduces a piecewise constant shaping function with goal of generalization across diverse architectures in large-scale settings, while our work exhibits superior generalization extending to small-scale settings too.

Training methods. The training methods incorporate adjustments during training to enhance the ID-OOD differentiating characteristics. They either make architectural adjustments (DeVries & Taylor, 2018; Hendrycks et al., 2019b; Hsu et al., 2020), apply enhanced data augmentations (Xiong et al., 2024; Hendrycks* et al., 2020; Hendrycks et al., 2022b), or make simple training modifications (Wei et al., 2022; Regmi et al., 2024a; Zhang et al., 2024). More recent methods have adopted contrastive learning in the context of OOD detection (Ming et al., 2023; Regmi et al., 2024b; Lu et al., 2024; Zou et al., 2025). Moreover, some approaches also either utilize external real outliers (Hendrycks et al., 2019a; Zhang et al., 2023b; Du et al., 2024; Zhu et al., 2023) or synthesize virtual outliers either in image space (Du et al., 2023; Regmi, 2024; Wang et al.,

2023; Gao et al., 2023; Zhang et al., 2025; Li et al., 2024; Bai et al., 2024; Nie et al., 2024) or in feature space (Du et al., 2022; Tao et al., 2023; Gao et al., 2024; Li & Zhang, 2025). However, training methods can be costlier and less effective than post-hoc approaches in some large-scale setups (Yang et al., 2022).

3. Preliminaries

Let \mathcal{X} denote the input space and $\mathcal{Y} = \{1, 2, \dots, C\}$ denote the label space, where C is the number of classes. We consider a multi-class classification setting where a classifier h is trained on ID data drawn from an underlying joint distribution $\mathcal{P}_{\text{ID}}(x, y)$, where $x \in \mathcal{X}$ and $y \in \mathcal{Y}$. The ID training dataset is denoted as $\mathcal{D}_{\text{ID}} = \{(x_i, y_i)\}_{i=1}^N$, where N is the number of training samples and $(x_i, y_i) \sim \mathcal{P}_{\text{ID}}(x, y)$. The classifier h is composed of a feature extractor $f_\theta : \mathcal{X} \rightarrow \mathcal{A} \in \mathbb{R}^D$, and a classifier $g_{\mathcal{W}} : \mathcal{A} \rightarrow \mathcal{Z} \in \mathbb{R}^C$. The feature extractor maps an input x to a feature vector $\mathbf{a} \in \mathcal{A}$, where $\mathbf{a} = f_\theta(x)$ and the classifier then maps this feature vector to a logit vector $\mathbf{z} = g_{\mathcal{W}}(\mathbf{a}) \in \mathbb{R}^C$. We refer to individual dimensions of the feature vector \mathbf{a} as activations, denoted by a_j for the j -th dimension. The classifier h is trained on \mathcal{D}_{ID} to minimize the empirical risk: $\min_{\theta, \mathcal{W}} \frac{1}{N} \sum_{i=1}^N \mathcal{L}(g_{\mathcal{W}}(f_\theta(x_i)), y_i)$ where \mathcal{L} is a loss function, such as cross-entropy loss. During inference, the model may encounter data points drawn from a different distribution, denoted as $\mathcal{P}_{\text{OOD}}(x)$, which is referred to as OOD data. The OOD detection problem aims to identify whether a given input x is drawn from marginal distribution $\mathcal{P}_{\text{ID}}(x)$ or from $\mathcal{P}_{\text{OOD}}(x)$. Hence, the goal is to design a scoring function $S(x) : \mathcal{X} \rightarrow \mathbb{R}$ that assigns a scalar score to each input x , reflecting its likelihood of being an OOD sample. A higher score typically indicates a higher probability of the input being OOD. A threshold τ is used to classify an input

$$\text{as either ID or OOD: } \text{OOD}(x) = \begin{cases} \text{True,} & \text{if } S(x) > \tau \\ \text{False,} & \text{if } S(x) \leq \tau \end{cases}.$$

4. Method

In this section, we introduce AdaSCALE, a novel post-processing approach that dynamically adapts the scaling mechanism based on each sample’s estimated OODness. We first revisit and analyze the core principle underlying recent scaling-based static state-of-the-art approaches. Then, we present our key empirical observations regarding activation behavior under minor perturbations, building upon insights from ReAct (Sun et al., 2021). Finally, we detail our proposed adaptive scaling mechanism that leverages these observations to achieve superior OOD detection performance.

4.1. Revisiting Static Scaling Mechanism

Scaling baselines (Djurisic et al., 2023; Xu et al., 2024; Djurisic et al., 2024) use energy score $-\log \sum_{i=1}^C e^{(\mathbf{z}_i)}$ on (directly or indirectly) scaled logits, with higher (magnitude) values indicating higher IDness. They operate by scaling activations / logits with scaling factor r , where $P_p(\mathbf{a})$ denotes p^{th} percentile of activation \mathbf{a} , computed as:

$$r = \frac{\sum_j \mathbf{a}_j}{\sum_{\mathbf{a}_j > P_p(\mathbf{a})} \mathbf{a}_j} \quad (1)$$

Pros analysis: They work well because of fusion of two independent and complementary OOD signals: activation patterns and original logits, where if one falls short, another can compensate leading to correct OOD detection signal.

Cons analysis: While this approach yields sample-specific scaling factors, it imposes a critical constraint: the p^{th} percentile threshold is static and identical across all test samples, regardless of the nature of samples. This static nature limits the effectiveness of the scaling procedure and prevents optimal ID-OOD separability.

Insights: Deeply analyzing both pros and cons, an insightful query naturally arises, “*Can we design another independent and complementary OOD signal and inject this signal through percentile, making it dynamic?*” For this, we study activation space to innovate the adaptive scaling mechanism.

4.2. Observations in Activation Space

A seminal work ReAct (Sun et al., 2021) demonstrated that OOD samples often induce abnormally high activations within neural networks. We extend this finding with an important observation: *the positions of such high activations in OOD samples are relatively unstable under minor perturbations compared to ID samples*. This instability provides a valuable signal for distinguishing OOD samples from ID samples. Below, we formalize this observation.

4.2.1. PERTURBATION MECHANISM

Let $x \in \mathbb{R}^{C_{\text{in}} \times H \times W}$ be an input image with C_{in} input channels, H height, and W width. We denote channel value at position (c, h, w) as $x[c, h, w]$. To identify channel values for perturbation, we employ pixel attribution that quantifies each input element’s influence on the model’s prediction. An attribution function, $AT(x, c, h, w)$, assigns a score to each channel value, with *lower* absolute scores indicating *less* influence. We select $o\%$ of channel value indices with *lowest* absolute attribution scores, forming the set R . We use a gradient-based attribution $AT(x, c, h, w) = \frac{\partial(g_w(f_\theta(x)))_{y_{\text{pred}}}}{\partial x[c, h, w]}$, where y_{pred} is predicted class index. To create a perturbed input, we select a subset R containing $o\%$ of channel values to perturb. If ε is

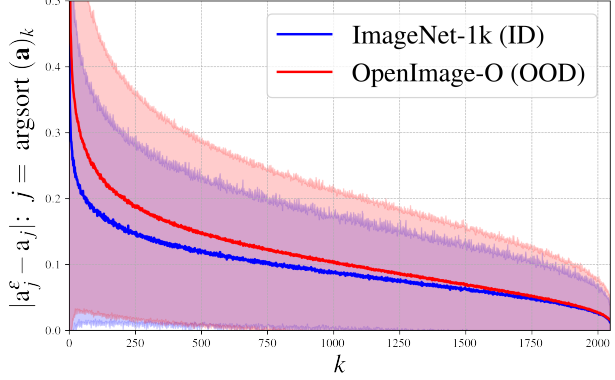


Figure 2. Activation shift comparison (with the mean denoted by a solid line and the standard deviation by a shaded region) between ID and OOD in the ResNet-50 model. The activation shift is significantly more pronounced in OOD samples compared to ID samples at high-magnitude activations (left side of the x-axis), providing a discriminative signal for OOD detection.

perturbation magnitude, perturbed image x^ε is obtained as:

$$x^\varepsilon[c, h, w] = \begin{cases} x[c, h, w] + \varepsilon \cdot \text{sign}(AT(x, c, h, w)), & \text{if } (c, h, w) \in R \\ x[c, h, w], & \text{if } (c, h, w) \notin R \end{cases} \quad (2)$$

Remark: Is attribution necessary for perturbation?

While we employ gradient-based attribution for principled pixel selection for perturbation, as we show later in Section F.5, it is important to note that even random selection empirically performs similarly, whereas selecting salient pixels degrades performance.

4.2.2. ACTIVATION SHIFT AS OOD INDICATOR

After obtaining perturbed input x^ε , we compute its activation $\mathbf{a}^\varepsilon = f_\theta(x^\varepsilon)$. We define *activation shift* as the absolute element-wise difference between original activation and the perturbed one:

$$\mathbf{a}^{\text{shift}} = |\mathbf{a}^\varepsilon - \mathbf{a}| \quad (3)$$

Figure 2 illustrates the key insight of our approach: activation shift at extreme (high-magnitude) activations is consistently more pronounced in OOD samples compared to ID samples. This behavior can be understood intuitively: ID samples activate network features in a stable, predictable manner reflecting learned patterns, while OOD samples trigger less stable, more arbitrary high activations that shift significantly under perturbation. Based on this observation, we propose using activation shift at the top- k_1 highest activations as a metric to estimate OODness of a sample:

$$Q = \sum_{j \in \text{argsort}(\mathbf{a}, \text{desc=True})[:k_1]} (|a_j^\varepsilon - a_j|) \quad (4)$$

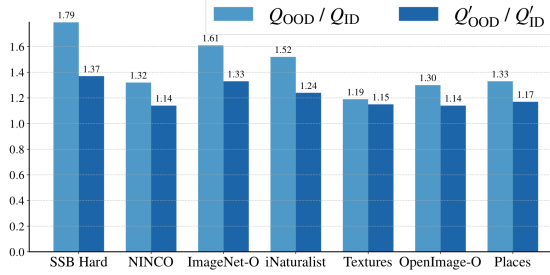


Figure 3. Q_{OOD}/Q_{ID} vs Q'_{OOD}/Q'_{ID} in various OOD datasets with ResNet-50 on ImageNet-1k. $Q'_{OOD}/Q'_{ID} < Q_{OOD}/Q_{ID}$ suggests C_o helps mitigate overconfident estimations.

where $\text{argsort}(\mathbf{a}, \text{desc} = \text{True})[: k_1]$ returns the indices of the k_1 highest values in \mathbf{a} . As evidenced by Q_{OOD}/Q_{ID} ratio (> 1) shown in Figure 3, the Q statistic generally assigns higher values to OOD samples than ID ones. However, the high variance of Q metric (Figure 2) suggests the possibility of overoptimistic estimations. To address this issue, we introduce a correction term C_o that exhibits an opposing behavior: it tends to be higher for ID samples than for OOD samples. Figure 5 in Section C shows that the perturbed activations of ID samples tend to be higher than those of OOD ones, especially in high-activation regions. We leverage this complementary signal by defining $C_o = \sum_{j \in \text{argsort}(\mathbf{a}, \text{desc}=\text{True})[:k_2]} \text{ReLU}(a_j^\varepsilon)$, where k_2 is a hyperparameter denoting the number of considered activations. We refine our OOD quantification by combining both metrics, weighted by a hyperparameter λ :

$$Q' = \lambda \cdot Q + C_o \quad (5)$$

The motivation behind Q' formulation instead of Q alone is to prevent the overconfident scaling factor from dominating the logit's contribution in the final energy score. (See Section D.1)

Indeed, Figure 3 illustrates that $Q'_{OOD}/Q'_{ID} < Q_{OOD}/Q_{ID}$, suggesting that the correction term C_o helps mitigate overconfident estimations. If $\bar{Q}_s = \{\bar{Q}'_1, \bar{Q}'_2, \dots, \bar{Q}'_{n_{val}}\}$ be the set of Q' values on n_{val} ID validation samples, we could transform any Q' into a normalized probability scale by constructing empirical cumulative distribution function (eCDF) derived from \bar{Q}_s . The eCDF, denoted as $F_{Q'}(Q')$, can be defined as:

$$F_{Q'}(Q') = \frac{1}{n_{val}} \sum_{i=1}^{n_{val}} \mathbb{1}(\bar{Q}'_i \leq Q') \quad (6)$$

where $\mathbb{1}(\cdot)$ is the indicator function. A higher value of $F_{Q'}(Q')$ indicates a higher likelihood of the sample being OOD. Importantly, our experiments suggest that as few as 10 ID validation samples are sufficient to construct an effective eCDF for this purpose (See Table 9).

Remark: ODIN vs. AdaSCALE in terms of perturbation

ODIN (Liang et al., 2018) perturbs entire image, inducing stronger confidence in ID inputs than OOD ones. In contrast, we apply trivial perturbations, perturbing only small number of trivial/random pixels to primarily compute shifts in top-k activations.

4.3. Proposed Approach: Adaptive Scaling

Building on our observations, we propose AdaSCALE (Adaptive SCALE), a novel approach that introduces dynamic, sample-specific adjustments to the scaling procedure. The key insight is that p^{th} percentile threshold should be a function of each test sample's estimated OODness rather than a fixed value. The scaling factor r increases as the p^{th} percentile threshold rises (i.e., when more activations are excluded from the denominator in Equation 1). For optimal ID-OOD separation, we must scale ID samples more strongly than OOD samples, requiring a higher p^{th} percentile for ID samples. We define an adaptive percentile threshold as:

$$p = p_{\min} + (1 - F_{Q'}(Q')) \cdot (p_{\max} - p_{\min}) \quad (7)$$

where p_{\min} and p_{\max} define the minimum and maximum limits of percentile threshold. It ensures samples with lower estimated OODness receive higher percentile thresholds, resulting in stronger scaling. (See Algorithm 1). We implement two variants: **AdaSCALE-A** scales activations as $\mathbf{a}_{\text{scaled}} = \mathbf{a} \cdot \exp(r)$ (Djurisic et al., 2023; Xu et al., 2024). **AdaSCALE-L** scales logits as $\mathbf{z}_{\text{scaled}} = \mathbf{z} \cdot r^2$ (Djurisic et al., 2024). This approach is also outlined in Figure 4.

5. Experiments

We use pre-trained models provided by PyTorch for ImageNet-1k experiments. For CIFAR experiments, we train three models per network using the standard cross-entropy loss and report the mean results across these three independent trials. The evaluation setup is provided in Table 1. The **non-percentile hyperparameters** ($\lambda = 10, k_1 = 1\%, k_2 = 5\%, o = 5\%, \epsilon = 0.5$) were **determined only once** using ResNet-50 model via OpenOOD's (Yang et al., 2022; Zhang et al., 2023c) automatic parameter search. We tune (p_{\min}, p_{\max}) for optimal results in each case (see Section H). However, near-optimal performance can be achieved by tuning only p_{\max} while fixing p_{\min} to 60 across all 22 cases (See Table 5) – difference is trivial. Best results are **bold**, and second-best results are underlined.

Metrics. We use two commonly used OOD Detection metrics: Area Under Receiver-Operator Characteristics (AUROC) and False Positive Rate at 95% True Positive Rate (FPR@95), where a higher AUROC and lower FPR@95 indicates better OOD detection performance.

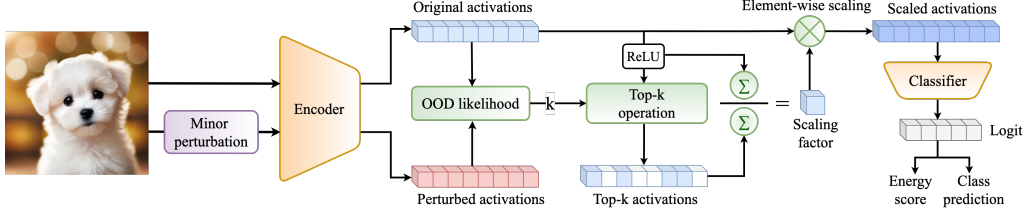


Figure 4. Schematic diagram of AdaSCALE’s working mechanism. AdaSCALE computes activation shifts between an original image and its slightly perturbed counterpart to estimate OODness. It, in-turn, determines an adaptive percentile threshold (p and thereby k), which controls the scaling factor r . Since r is defined as the ratio of total activation sum to the sum of activations above the percentile threshold, samples with higher OODness receive lower scaling factors. This adaptive approach yields highly separable energy scores that enable effective OOD detection.

Table 1. Experimental evaluation setup for OOD detection.

Conventional OOD detection			
ID datasets	Near-OOD	Far-OOD	Network
CIFAR-10/100	CIFAR-100/10 TIN	MNIST, SVHN, Textures, Places365	WRN-28-10, DenseNet-101
ImageNet-1k	SSB-Hard	iNaturalist,	EfficientNetV2-L, ResNet-101
	NINCO	OpenImage-O	DenseNet-201, ViT-B-16
	ImageNet-O	Textures Places	ResNet-50, ResNeXt-50 RegNet-Y-16, Swin-B
Covariate shifted datasets for full spectrum OOD detection			
ImageNet-1k	ImageNet-C, ImageNet-R, ImageNet-V2, ImageNet-ES		

Baselines. MSP, EBO, ReAct, MLS, ASH, SCALE, BFAct, LTS, OptFS. See Section D.3 for additional comparisons. Currently, SCALE is the *best-performing* method (with ResNet-50), while OptFS is the *best-generalizing* method.

5.1. Empirical Results

Table 2. OOD detection results (FPR@95 \downarrow / AUROC \uparrow) averaged over WRN-28-10 and DenseNet-101 on CIFAR benchmarks across 3 trials. (See Section I for complete results.)

Method	CIFAR-10		CIFAR-100	
	Near-OOD	Far-OOD	Near-OOD	Far-OOD
MSP	43.18 / 89.07	34.49 / 90.88	55.64 / 80.23	61.73 / 76.82
MLS	51.54 / 89.33	39.62 / 91.68	57.24 / 81.25	60.19 / 78.92
EBO	51.54 / 89.37	39.58 / 91.75	57.45 / 81.10	60.12 / 78.96
ReAct	49.71 / 88.59	37.32 / 92.00	63.20 / 79.58	54.78 / 80.46
ASH	78.11 / 77.97	63.12 / 83.35	80.97 / 70.09	69.38 / 79.06
SCALE	53.00 / 89.20	39.27 / 91.93	58.38 / 81.00	57.19 / 80.56
BFAct	54.90 / 88.56	43.05 / 90.66	72.26 / 74.70	57.44 / 77.63
LTS	55.71 / 88.77	41.06 / 91.74	59.98 / 80.60	80.48 / 81.79
OptFS	64.82 / 85.72	47.67 / 89.99	76.80 / 73.02	60.23 / 77.76
AdaSCALE-A	43.07 / 90.31	33.11 / 92.66	57.33 / 81.35	54.53 / 81.14
AdaSCALE-L	44.71 / 90.14	33.43 / 92.69	58.70 / 81.07	52.49 / 82.21

CIFAR benchmark. We compare AdaSCALE with post-hoc baselines on CIFAR benchmarks using WRN-28-10 and DenseNet-101 networks, reporting the averaged performance in Table 2. AdaSCALE outperforms all methods in average AUROC metric across CIFAR benchmarks in both near- and far-OOD detection. For far-OOD detection on CIFAR-10 benchmark, AdaSCALE-A achieves the best FPR@95 score of **33.11**, outperforming the MSP baseline by approximately 1.4 points. Similarly, AdaSCALE-A attains the best FPR@95 / AUROC of **43.07 / 90.31** in near-

OOD detection, though MSP remains competitive. In near-OOD detection on CIFAR-100 benchmark, AdaSCALE-A achieves the highest AUROC of **81.35**, while in far-OOD detection, AdaSCALE-L reaches the best performance with FPR@95 / AUROC of **52.49 / 82.21**. While activation-shaping methods perform well in ImageNet-1k, they seem to underperform in CIFAR. In contrast, AdaSCALE achieves consistently superior performance across all setups.

ImageNet-1k benchmark. We compare our proposed method, AdaSCALE, with recent state-of-the-art approaches across eight architectures on the ImageNet-1k benchmark, as presented in Table 3. AdaSCALE demonstrates consistently strong performance across all architectures compared to existing methods. Specifically, it surpasses the *best-generalizing* method, OptFS, by **14.94% / 8.96%** in the FPR@95/AUROC metric for near-OOD detection across all architectures. Additionally, it outperforms the *best-performing* method, SCALE (on ResNet-50), by **12.96% / 6.44%** in the same metric. A closer observation reveals that while OptFS excels in architectures such as EfficientNet, ViT-B-16, and Swin-B, scaling baselines perform comparably or even better in architectures like ResNet-50, ResNet-101, RegNet-Y-16, and DenseNet-201. In contrast, AdaSCALE-A achieves the best performance in near-OOD detection across all architectures, except for Swin-B, where BFAct performs optimally. Furthermore, effectiveness of AdaSCALE extends beyond near-OOD detection to far-OOD detection, demonstrating an average gain of **21.67%** over OptFS in the FPR@95 metric.

FSOOD Detection.

FSOOD detection extends conventional OOD detection by incorporating model’s ability to generalize on covariate-shifted ID inputs. We present FSOOD detection results in Table 4 in FPR@95 \downarrow / AUROC \uparrow format. We can observe that this is

Table 4. Avg. FSOOD detection on ImageNet-1k over 8 architectures.

Method	Near-OOD	Far-OOD
ReAct	87.22 / 51.38	67.23 / 69.53
ASH	87.01 / 52.02	72.36 / 65.70
SCALE	86.75 / 52.27	69.36 / 68.97
BFAct	87.12 / 51.14	66.13 / 69.69
LTS	86.46 / 53.29	66.76 / 71.63
OptFS	85.83 / 52.17	63.32 / 71.44
AdaSCALE-A	81.34 / 55.03	58.87 / 72.41
AdaSCALE-L	81.62 / 55.14	59.19 / 72.85

Table 3. OOD detection results (FPR@95 \downarrow / AUROC \uparrow) on ImageNet-1k benchmark.

Method	ResNet-50	ResNet-101	RegNet-Y-16	ResNeXt-50	DenseNet-201	EfficientNetV2-L	ViT-B-16	Swin-B	Average	
near-OOD	MSP	74.23 / 60.21	71.96 / 67.25	62.22 / 80.74	73.25 / 67.86	73.44 / 67.29	72.51 / 80.76	86.72 / 68.62	87.11 / 69.82	75.18 / 70.32
	MLS	74.87 / 64.55	72.05 / 71.51	62.94 / 84.66	74.11 / 71.62	75.51 / 68.91	81.44 / 79.22	93.78 / 63.64	94.80 / 64.68	78.69 / 71.10
	EBO	75.32 / 64.52	72.32 / 71.54	62.80 / 84.76	74.21 / 71.61	75.85 / 68.68	82.86 / 77.15	94.37 / 59.19	95.34 / 59.79	79.13 / 69.66
	ReAct	72.61 / 68.81	68.07 / 75.00	70.73 / 75.37	70.96 / 74.13	69.97 / 73.65	72.36 / 71.39	86.63 / 68.35	82.64 / 73.26	74.25 / 72.50
	ASH	69.47 / 71.33	65.24 / 76.61	82.51 / 67.81	70.98 / 75.25	92.83 / 52.30	94.85 / 44.78	94.45 / 53.20	96.37 / 47.58	83.34 / 61.11
	SCALE	67.76 / 74.20	63.87 / 78.60	67.09 / 82.90	70.59 / 76.20	71.56 / 73.72	89.70 / 60.12	94.48 / 56.18	88.62 / 61.47	76.71 / 70.42
	BFact	72.35 / 68.88	67.96 / 75.16	78.72 / 66.09	70.96 / 74.14	71.20 / 72.61	75.53 / 62.46	82.09 / 70.66	71.81 / 75.28	73.83 / 70.66
	LTS	68.01 / 73.37	63.91 / 78.27	69.82 / 80.75	70.27 / 76.20	71.29 / 74.56	87.30 / 73.63	88.83 / 67.43	86.61 / 67.22	75.76 / 73.93
	OptFS	69.66 / 70.97	65.46 / 75.83	73.53 / 75.21	69.27 / 74.84	71.74 / 72.10	72.29 / 75.29	76.55 / 72.73	76.81 / 74.06	71.91 / 73.88
far-OOD	AdaSCALE-A	58.98 / 78.98	57.96 / 81.68	47.91 / 89.18	64.14 / 79.96	61.28 / 79.66	53.78 / 86.94	71.87 / 73.14	73.41 / 74.48	61.17 / 80.50
	AdaSCALE-L	59.84 / 78.62	56.41 / 81.86	56.13 / 87.11	62.08 / 80.18	61.75 / 80.06	54.95 / 85.77	71.99 / 73.23	72.89 / 74.58	62.00 / 80.18
	MSP	53.15 / 84.06	53.87 / 83.81	40.41 / 90.08	53.07 / 84.21	53.60 / 84.43	54.74 / 87.92	56.41 / 84.62	73.39 / 82.02	54.83 / 85.14
	MLS	42.57 / 88.19	43.89 / 88.30	32.92 / 93.70	44.91 / 87.97	48.43 / 87.44	68.64 / 84.80	81.89 / 81.42	95.16 / 73.37	57.30 / 85.65
	EBO	42.72 / 88.09	44.30 / 88.23	32.47 / 93.82	45.12 / 87.86	48.95 / 87.15	74.48 / 81.13	86.95 / 76.34	96.08 / 63.99	58.88 / 83.33
	ReAct	30.14 / 92.98	29.89 / 93.10	45.20 / 86.17	30.06 / 92.69	30.72 / 92.65	60.05 / 75.33	59.31 / 83.65	58.86 / 84.77	43.03 / 87.67
	ASH	24.69 / 94.43	26.18 / 94.06	59.65 / 83.94	29.17 / 93.47	33.50 / 92.17	96.56 / 41.57	95.98 / 52.16	98.23 / 43.20	57.99 / 74.38
	SCALE	21.44 / 95.39	22.54 / 95.05	32.16 / 94.16	30.62 / 93.54	33.17 / 92.70	89.63 / 62.58	88.36 / 72.32	86.59 / 66.77	50.56 / 84.06
	BFact	29.46 / 93.01	29.43 / 93.04	58.69 / 77.22	29.71 / 92.67	32.45 / 92.29	66.72 / 65.70	51.58 / 85.77	38.99 / 88.47	42.13 / 86.02
	LTS	22.20 / 95.24	23.07 / 94.94	34.99 / 93.57	30.37 / 93.49	30.92 / 93.29	86.85 / 76.30	64.37 / 84.43	85.84 / 44.80	47.33 / 84.51
	OptFS	25.66 / 93.87	26.97 / 93.55	47.37 / 86.73	27.54 / 93.40	34.42 / 91.04	53.62 / 83.62	46.11 / 87.35	44.27 / 87.79	38.25 / 89.67
AdaSCALE-A	17.84 / 96.14	18.51 / 95.95	21.37 / 95.84	22.08 / 95.24	28.01 / 93.23	37.61 / 91.48	47.63 / 86.83	47.81 / 87.14	30.11 / 92.73	
	AdaSCALE-L	17.92 / 96.12	19.15 / 95.76	20.10 / 96.19	22.16 / 95.01	28.00 / 93.18	38.81 / 90.51	47.28 / 86.97	46.24 / 87.97	29.96 / 92.71

a challenging task, as covariate-shifted ID datasets cause significant performance drop for all methods compared to conventional case. Yet, AdaSCALE outperforms OptFS by **4.49** and **4.13** points on average in FPR@95 for FSOOD detection across both near- and far-OOD datasets.

Accuracy: Like SCALE & LTS, AdaSCALE applies linear transformations to scale activations or logits, preserving accuracy, unlike post-hoc rectification methods (ASH, ReAct).

5.2. Ablation / Hyperparameter studies / Discussion

Table 5. Tuning just one hyperparameter p_{\max} is enough for superior generalization of AdaSCALE over OptFS.

Method	ImageNet-1k		CIFAR-100	
	Near-OOD	Far-OOD	Near-OOD	Far-OOD
OptFS	71.91 / 73.88	38.25 / 89.67	76.81 / 73.02	60.23 / 77.76
AdaSCALE-A	62.29 / 79.72	32.72 / 91.82	58.00 / 81.14	56.47 / 80.99

Constrained hyperparameter tuning. The hyperparameters $(\lambda, k_1, k_2, o, \epsilon) = (10, 1\%, 5\%, 5\%, 0.5)$ determined with a ResNet-50 in ImageNet-1k benchmark generalize across architectures and datasets. To demonstrate this, we conduct experiments only allowing p_{\max} to be tuned across 8 and 2 architectures in ImageNet-1k and CIFAR-100 datasets, respectively and present the results in Table 5. Inspired by early works that tune the percentile hyperparameter in [60, 99], we set p_{\min} to lower limit 60. Even under this highly constrained setting, AdaSCALE significantly outperforms the previous state-of-the-art (OptFS) by an average of **13%** (FPR95) / **8%** (AUROC) on near-OOD and **14%** (FPR@95) / **2%** (AUROC) on far-OOD datasets on ImageNet-1k benchmark. The superiority of AdaSCALE over OptFS is also evident in a small-scale setting (CIFAR-100).

Robustness analysis. We evaluate the practical robustness

Table 6. Robustness analysis with ResNet-50 in ImageNet-1k.

Metric / Method	Gaussian blur	JPEG compression	Adversarial training
FPR@95 \downarrow (Near-OOD / Far-OOD)			
SCALE	72.68 / 29.65	69.73 / 27.46	66.99 / 24.77
OptFS	71.84 / 30.27	69.43 / 28.34	70.11 / 28.32
AdaSCALE-A	67.53 / 28.11	61.24 / 25.87	60.21 / 21.13
AUROC \uparrow (Near-OOD / Far-OOD)			
SCALE	70.15 / 92.72	71.84 / 93.56	76.10 / 94.40
OptFS	69.66 / 92.24	71.12 / 92.95	73.51 / 93.42
AdaSCALE-A	75.18 / 93.31	77.59 / 94.06	80.68 / 95.35

of AdaSCALE under both real-world image corruptions and adversarial training. Specifically, we compare AdaSCALE against SCALE and OptFS on ImageNet-1k using a ResNet-50, applying Gaussian blur (kernel=5, $\sigma \in (0.01, 0.5)$) and JPEG compression (50%) to the input images, without any hyperparameter re-tuning. In addition, we evaluate AdaSCALE on an adversarially trained ResNet-50 ($\epsilon = 0.05$) using the same hyperparameters as in the standard setting. The results (Near-OOD / Far-OOD), shown in Table 6, demonstrate that AdaSCALE consistently outperforms SCALE and OptFS, indicating robustness across both input perturbations and diverse training schemes.

Sensitivity study. We study sensitivity of AdaSCALE-A hyperparameters with ResNet-50 on ImageNet-1k (Table 7). The optimal perturbation magnitude is $\epsilon = 0.5$, close to RGB means and sufficient to disturb peak activations. Furthermore, setting $\lambda = 10$ ensures activation shift Q dominates the regularizer C_o . Optimal performance at $k_1 = 1\%$ confirms that shifts in peak activations are the most reliable OOD signal, while $k_2 = 5\%$ empirically performs best. $o = 5\%$ yielding optimal result supports our hypothesis that perturbation should be trivial enough to only disturb peak activations. (See Sections E and F for complete study.)

How effective is Q without scaling? As shown in Figure 2,

Table 7. Sensitivity study (FPR@95 \downarrow / AUROC \uparrow) with ResNet-50 model on ImageNet-1k benchmark.

ϵ	Near-OOD	Far-OOD	λ	Near-OOD	Far-OOD	k_1	Near-OOD	Far-OOD	k_2	Near-OOD	Far-OOD	o	Near-OOD	Far-OOD
0.1	63.76 / 77.50	19.26 / 95.85	1	67.49 / 75.45	20.41 / 95.54	1%	58.97 / 78.98	17.84 / 96.14	1%	59.08 / 78.56	18.35 / 96.02	1%	61.77 / 78.29	19.28 / 95.77
0.5	58.97 / 78.98	17.84 / 96.14	10	58.97 / 78.98	17.84 / 96.14	10%	60.40 / 77.89	19.72 / 95.63	5%	58.97 / 78.98	17.84 / 96.14	5%	58.97 / 78.98	17.84 / 96.14
1.0	61.60 / 76.96	19.31 / 95.84	100	59.03 / 78.10	19.39 / 95.80	100%	60.99 / 76.49	21.88 / 94.96	100%	62.43 / 75.44	23.05 / 94.69	100%	67.37 / 73.08	22.93 / 95.01

Q alone, without scaling, is not sufficiently discriminative. Its value lies in providing an independent and complementary OOD detection signal that is distinct from activation-pattern and logit-based information. For example, when Q is directly used for near-OOD scoring on ImageNet-1k benchmark with ResNet-50, it achieves an FPR@95 \downarrow / AUROC \uparrow of 79.81/72.32. In contrast, incorporating Q into the scaling mechanism substantially improves performance to 59.43/78.14. Hence, Q alone is not effective.

 Table 8. Comparison between Q' and Q in average OOD detection performance on ImageNet-1k benchmark over 8 architectures.

Metric	Near-OOD	Far-OOD
Q	68.90 / 78.07	42.63 / 89.18
Q'	61.17 / 80.50	30.11 / 92.73

Is Q' really needed instead of Q ? Yes. AdaSCALE integrates three independent sources of OOD evidence – activation patterns, logit information, and activation shift – none of which serves as an oracle on its own. While Q (activation shift) captures feature-level instability, relying on it alone without a balancing mechanism can lead to large scaling factors that overwhelm the informative OOD signal present in the logits. By incorporating the balancing term C_o , Q' appropriately regulates the influence of activation shift and preserves the contribution of logit information for OOD detection. This design choice is empirically validated on ImageNet-1k benchmark in Table 8. (See Section D.1).

Why does AdaSCALE outperform OptFS? OptFS applies interval-specific activation scaling which yields *modified* logits used for OOD scoring. While this can improve separability on average, it implicitly assumes that activation reshaping is beneficial for every sample. For near-OOD inputs with ID-like activation patterns, this reshaping can distort informative *original* logit signals and lead to suboptimal OOD detection. (See Section J for dataset-specific results for OptFS on the SSB-Hard datasets). AdaSCALE avoids this rigidity by adaptively fusing multiple, partially independent OOD cues allowing alternative signals to compensate when one becomes unreliable.

ID statistics. With the rise of large models, where training data is often undisclosed or inaccessible, relying on full

training ID datasets for OOD detection has become increasingly impractical. We rigorously assess AdaSCALE’s effectiveness with limited data by conducting experiments on ImageNet-1k with ResNet-50 using n_{val} ID samples to compute ID statistics, where $n_{\text{val}} \in \{10, 100, 1000, 5000\}$. The results (FPR@95 \downarrow / AUROC \uparrow) in Table 9 confirm that even with substantially restricted access to ID data, AdaSCALE-A achieves state-of-the-art performance.

Table 10. Latency with fixed vs. variable percentile.

Percentile	$D = 128$	$D = 512$	$D = 1024$	$D = 2048$	$D = 3024$
Fixed (SCALE/LTS)	33 μ s	40 μ s	45 μ s	48 μ s	54 μ s
Variable (AdaSCALE)	152 μ s	149 μ s	155 μ s	152 μ s	164 μ s
Latency ratio (AdaSCALE / SCALE)	4.66	3.76	3.42	3.14	3.02

Latency. AdaSCALE requires an additional forward pass to compute the perturbed activation \mathbf{a}^ϵ only when gradient-based pixel perturbation is used; random perturbation, does not incur this cost. Also, top-k operations (time complexity: $\mathcal{O}(D \log D)$) are applied to Q and C_o to estimate OODness. Comparing variable vs. fixed percentiles for scaling in Table 10 over 10,000 trials, we observe that variable percentiles induce higher latency, though the latency ratio decreases with higher-dimensional activation spaces. While SCALE and OptFS have similar latency, AdaSCALE’s is 2.91x higher with gradient attribution for trivial pixel perturbation, dropping to 1.56x with random pixel perturbation.

6. Conclusion

We propose **AdaSCALE**, a novel post-hoc OOD detection method that dynamically adjusts scaling process based on a sample’s estimated OODness. Leveraging the observation that OOD samples exhibit larger activation shifts under minor perturbations, AdaSCALE assigns stronger scaling to likely ID samples and weaker scaling to likely OOD samples, enhancing ID-OOD separability. AdaSCALE achieves state-of-the-art performance as well as generalization across architectures requiring negligibly few ID samples, making it highly practical for real-world deployment. To sum up, it moves scaling-based OOD detection from heuristic-based to a more principled footing.

Impact Statement

This paper presents work whose goal is to advance the field of Machine Learning. There are many potential societal consequences of our work, none of which we feel must be specifically highlighted here.

References

Ahn, Y. H., Park, G.-M., and Kim, S. T. Line: Out-of-distribution detection by leveraging important neurons. In *Proceedings of the IEEE/CVF Conference on Computer Vision and Pattern Recognition (CVPR)*, pp. 19852–19862, June 2023.

Ammar, M. B., Belkhir, N., Popescu, S., Manzanera, A., and Franchi, G. NECO: NEural collapse based out-of-distribution detection. In *The Twelfth International Conference on Learning Representations (ICLR)*, 2024. URL <https://openreview.net/forum?id=9ROuKb1mi7>.

Baek, E., Park, K., Kim, J., and Kim, H.-S. Unexplored faces of robustness and out-of-distribution: Covariate shifts in environment and sensor domains. In *Proceedings of the IEEE/CVF Conference on Computer Vision and Pattern Recognition (CVPR)*, pp. 22294–22303, 2024.

Bai, Y., Han, Z., Cao, B., Jiang, X., Hu, Q., and Zhang, C. Id-like prompt learning for few-shot out-of-distribution detection. In *Proceedings of the IEEE/CVF Conference on Computer Vision and Pattern Recognition (CVPR)*, pp. 17480–17489, June 2024.

Behpour, S., Doan, T., Li, X., He, W., Gou, L., and Ren, L. Gradorth: A simple yet efficient out-of-distribution detection with orthogonal projection of gradients. In *Thirty-seventh Conference on Neural Information Processing Systems (NeurIPS)*, 2023. URL <https://openreview.net/forum?id=L9nTuSbAws>.

Chen, J., Li, J., Qu, X., Wang, J., Wan, J., and Xiao, J. GAIA: Delving into gradient-based attribution abnormality for out-of-distribution detection. In *Thirty-seventh Conference on Neural Information Processing Systems (NeurIPS)*, 2023. URL <https://openreview.net/forum?id=XEBzQP3e7B>.

DeVries, T. and Taylor, G. W. Learning confidence for out-of-distribution detection in neural networks. *arXiv preprint arXiv:1802.04865*, 2018.

Djurisic, A., Bozanic, N., Ashok, A., and Liu, R. Extremely simple activation shaping for out-of-distribution detection. In *The Eleventh International Conference on Learning Representations (ICLR)*, 2023.

Djurisic, A., Liu, R., and Nikolic, M. Logit scaling for out-of-distribution detection. *arXiv preprint arXiv:2409.01175*, 2024.

Du, X., Wang, Z., Cai, M., and Li, Y. Vos: Learning what you don't know by virtual outlier synthesis. In *Proceedings of the International Conference on Learning Representations (ICLR)*, 2022.

Du, X., Sun, Y., Zhu, J., and Li, Y. Dream the impossible: Outlier imagination with diffusion models. *Advances in Neural Information Processing Systems (NeurIPS)*, 36: 60878–60901, 2023.

Du, X., Fang, Z., Diakonikolas, I., and Li, Y. How does unlabeled data provably help out-of-distribution detection? In *The Twelfth International Conference on Learning Representations (ICLR)*, 2024. URL <https://openreview.net/forum?id=j1EjB8MVGa>.

Gao, H., He, Z., Qiu, S., and Pu, J. Oal: Enhancing ood detection using latent diffusion, 2024. URL <https://arxiv.org/abs/2406.16525>.

Gao, R., Zhao, C., Hong, L., and Xu, Q. Diffguard: Semantic mismatch-guided out-of-distribution detection using pre-trained diffusion models. In *Proceedings of the IEEE/CVF International Conference on Computer Vision (ICCV)*, pp. 1579–1589, October 2023.

Granz, M., Heurich, M., and Landgraf, T. Weiper: OOD detection using weight perturbations of class projections. In *The Thirty-eighth Annual Conference on Neural Information Processing Systems (NeurIPS)*, 2024. URL <https://openreview.net/forum?id=8HeUvbImKT>.

He, R., Yuan, Y., Han, Z., Wang, F., Su, W., Yin, Y., Liu, T., and Gong, Y. Exploring channel-aware typical features for out-of-distribution detection. In *Proceedings of the AAAI conference on artificial intelligence (AAAI)*, volume 38, pp. 12402–12410, 2024.

Hendrycks, D. and Gimpel, K. A baseline for detecting misclassified and out-of-distribution examples in neural networks. In *International Conference on Learning Representations (ICLR)*, 2017.

Hendrycks, D., Mazeika, M., and Dietterich, T. Deep anomaly detection with outlier exposure. In *International Conference on Learning Representations (ICLR)*, 2019a.

Hendrycks, D., Mazeika, M., Kadavath, S., and Song, D. Using self-supervised learning can improve model robustness and uncertainty. In *Proceedings of the 33rd Conference on Neural Information Processing Systems (NeurIPS)*, 2019b.

Hendrycks*, D., Mu*, N., Cubuk, E. D., Zoph, B., Gilmer, J., and Lakshminarayanan, B. Augmix: A simple method to improve robustness and uncertainty under data shift. In *International Conference on Learning Representations (ICLR)*, 2020. URL <https://openreview.net/forum?id=S1gmrxHFvB>.

Hendrycks, D., Basart, S., Mazeika, M., Mostajabi, M., Steinhardt, J., and Song, D. Scaling out-of-distribution detection for real-world settings. In *International Conference on Machine Learning (ICML)*, 2022a.

Hendrycks, D., Zou, A., Mazeika, M., Tang, L., Li, B., Song, D., and Steinhardt, J. Pixmix: Dreamlike pictures comprehensively improve safety measures. In *Proceedings of the IEEE/CVF Conference on Computer Vision and Pattern Recognition (CVPR)*, pp. 16783–16792, June 2022b.

Hsu, Y.-C., Shen, Y., Jin, H., and Kira, Z. Generalized odin: Detecting out-of-distribution image without learning from out-of-distribution data. In *Proceedings of the IEEE/CVF Conference on Computer Vision and Pattern Recognition (CVPR)*, 2020.

Huang, R., Geng, A., and Li, Y. On the importance of gradients for detecting distributional shifts in the wild. *Advances in Neural Information Processing Systems (NeurIPS)*, 34, 2021.

Kim, J.-H., Yun, S., and Song, H. O. Neural relation graph: a unified framework for identifying label noise and outlier data. *Advances in Neural Information Processing Systems (NeurIPS)*, 36, 2024.

Kong, H. and Li, H. Bfact: Out-of-distribution detection with butterworth filter rectified activations. In *International Conference on Cognitive Systems and Signal Processing (ICCSIP)*, pp. 115–129. Springer, 2022.

Krumpl, G., Avenhaus, H., Possegger, H., and Bischof, H. Ats: Adaptive temperature scaling for enhancing out-of-distribution detection methods. In *Proceedings of the IEEE/CVF Winter Conference on Applications of Computer Vision (WACV)*, pp. 3864–3873, January 2024.

Lee, K., Lee, K., Lee, H., and Shin, J. A simple unified framework for detecting out-of-distribution samples and adversarial attacks. In *Advances in Neural Information Processing Systems (NeurIPS)*, 2018.

Li, H. and Zhang, T. Outlier synthesis via hamiltonian monte carlo for out-of-distribution detection. In *The Thirteenth International Conference on Learning Representations (ICLR)*, 2025. URL <https://openreview.net/forum?id=N6ba2xsmds>.

Li, T., Pang, G., Bai, X., Miao, W., and Zheng, J. Learning transferable negative prompts for out-of-distribution detection. In *Proceedings of the IEEE/CVF Conference on Computer Vision and Pattern Recognition (CVPR)*, pp. 17584–17594, June 2024.

Liang, S., Li, Y., and Srikant, R. Enhancing the reliability of out-of-distribution image detection in neural networks. In *International Conference on Learning Representations (ICLR)*, 2018.

Liu, L. and Qin, Y. Detecting out-of-distribution through the lens of neural collapse. *arXiv preprint arXiv:2311.01479*, 2023.

Liu, L. and Qin, Y. Fast decision boundary based out-of-distribution detector. In *International Conference on Machine Learning (ICML)*, 2024.

Liu, W., Wang, X., Owens, J. D., and Li, Y. Energy-based out-of-distribution detection. In *Proceedings of the 34th Conference on Neural Information Processing Systems (NeurIPS)*, 2020.

Liu, X., Lochman, Y., and Zach, C. Gen: Pushing the limits of softmax-based out-of-distribution detection. In *Proceedings of the IEEE/CVF Conference on Computer Vision and Pattern Recognition*, 2023.

Lu, H., Gong, D., Wang, S., Xue, J., Yao, L., and Moore, K. Learning with mixture of prototypes for out-of-distribution detection. In *The Twelfth International Conference on Learning Representations (ICLR)*, 2024.

Ming, Y., Sun, Y., Dia, O., and Li, Y. How to exploit hyperspherical embeddings for out-of-distribution detection? In *The Eleventh International Conference on Learning Representations (ICLR)*, 2023.

Nie, J., Luo, Y., Ye, S., Zhang, Y., Tian, X., and Fang, Z. Out-of-distribution detection with virtual outlier smoothing. *International Journal of Computer Vision (IJCV)*, 2024.

Olber, B., Radlak, K., Popowicz, A., Szczechankiewicz, M., and Chachula, K. Detection of out-of-distribution samples using binary neuron activation patterns. In *Proceedings of the IEEE/CVF Conference on Computer Vision and Pattern Recognition (CVPR)*, 2023.

Park, J., Jung, Y. G., and Teoh, A. B. J. Nearest neighbor guidance for out-of-distribution detection. In *Proceedings of the IEEE/CVF International Conference on Computer Vision*, 2023.

Rajasekaran, M., Sajol, M. S. I., Berglind, F., Mukhopadhyay, S., and Das, K. Combood: A semiparametric approach for detecting out-of-distribution data for image classification. In *Proceedings of the 2024 SIAM International Conference on Data Mining (SDM)*, pp. 643–651. SIAM, 2024.

Regmi, S. Going beyond conventional ood detection, 2024.

Regmi, S., Panthi, B., Dotel, S., Gyawali, P. K., Stoyanov, D., and Bhattacharai, B. T2fnorm: Train-time feature normalization for ood detection in image classification. In *Proceedings of the IEEE/CVF Conference on Computer Vision and Pattern Recognition (CVPR) Workshops*, 2024a.

Regmi, S., Panthi, B., Ming, Y., Gyawali, P. K., Stoyanov, D., and Bhattacharai, B. Reweightingood: Loss reweighting for distance-based ood detection. In *Proceedings of the*

IEEE/CVF Conference on Computer Vision and Pattern Recognition (CVPR) Workshops, 2024b.

Ren, J., Fort, S., Liu, J., Roy, A. G., Padhy, S., and Lakshminarayanan, B. A simple fix to mahalanobis distance for improving near-ood detection. *arXiv preprint arXiv:2106.09022*, 2021.

Sharifi, S., Entesari, T., Safaei, B., Patel, V. M., and Fazlyab, M. Gradient-regularized out-of-distribution detection. In Leonardis, A., Ricci, E., Roth, S., Russakovsky, O., Sattler, T., and Varol, G. (eds.), *European Conference on Computer Vision (ECCV)*, pp. 691–708, Cham, 2025. Springer.

Sun, Y. and Li, Y. Dice: Leveraging sparsification for out-of-distribution detection. In *European Conference on Computer Vision (ECCV)*, pp. 691–708. Springer, 2022.

Sun, Y., Guo, C., and Li, Y. React: Out-of-distribution detection with rectified activations. *Advances in Neural Information Processing Systems (NeurIPS)*, 34, 2021.

Sun, Y., Ming, Y., Zhu, X., and Li, Y. Out-of-distribution detection with deep nearest neighbors. *Proceedings of the 39th International Conference on Machine Learning (ICML)*, 2022.

Tao, L., Du, X., Zhu, J., and Li, Y. Non-parametric outlier synthesis. In *The Eleventh International Conference on Learning Representations (ICLR)*, 2023.

Wang, H., Li, Z., Feng, L., and Zhang, W. Vim: Out-of-distribution with virtual-logit matching. In *Proceedings of the IEEE/CVF Conference on Computer Vision and Pattern Recognition (CVPR)*, 2022.

Wang, H., Li, Y., Yao, H., and Li, X. Clipn for zero-shot ood detection: Teaching clip to say no. In *Proceedings of the IEEE/CVF International Conference on Computer Vision (ICCV)*, pp. 1802–1812, October 2023.

Wei, H., Xie, R., Cheng, H., Feng, L., An, B., and Li, Y. Mitigating neural network overconfidence with logit normalization. In *International Conference on Machine Learning (ICML)*. PMLR, 2022.

Xiong, H., Xu, K., and Yao, A. Fixing data augmentations for out-of-distribution detection, 2024. URL <https://openreview.net/forum?id=1ebgtm7P10>.

Xu, K., Chen, R., Franchi, G., and Yao, A. Scaling for training time and post-hoc out-of-distribution detection enhancement. In *The Twelfth International Conference on Learning Representations (ICLR)*, 2024.

Xu, M., Lian, Z., Liu, B., and Tao, J. Vra: Variational rectified activation for out-of-distribution detection. *Advances in Neural Information Processing Systems (NeurIPS)*, 2023.

Xu, P., Ehinger, K. A., Zhang, Y., Finkelstein, A., Kulkarni, S. R., and Xiao, J. Turkergaze: Crowdsourcing saliency with webcam based eye tracking. *arXiv preprint arXiv:1504.06755*, 2015.

Yang, J., Wang, P., Zou, D., Zhou, Z., Ding, K., Peng, W., Wang, H., Chen, G., Li, B., Sun, Y., Du, X., Zhou, K., Zhang, W., Hendrycks, D., Li, Y., and Liu, Z. OpenOOD: Benchmarking generalized out-of-distribution detection. In *Advances in Neural Information Processing Systems (NeurIPS), Datasets and Benchmarks Track*, 2022.

Yang, J., Zhou, K., and Liu, Z. Full-spectrum out-of-distribution detection. *International Journal of Computer Vision (IJCV)*, 2023.

Zhang, J., Fu, Q., Chen, X., Du, L., Li, Z., Wang, G., xi-aoguang Liu, Han, S., and Zhang, D. Out-of-distribution detection based on in-distribution data patterns memorization with modern hopfield energy. In *The Eleventh International Conference on Learning Representations (ICLR)*, 2023a.

Zhang, J., Inkawich, N., Linderman, R., Chen, Y., and Li, H. Mixture outlier exposure: Towards out-of-distribution detection in fine-grained environments. In *Proceedings of the IEEE/CVF Winter Conference on Applications of Computer Vision (WACV)*, 2023b.

Zhang, J., Yang, J., Wang, P., Wang, H., Lin, Y., Zhang, H., Sun, Y., Du, X., Zhou, K., Zhang, W., et al. Openood v1.5: Enhanced benchmark for out-of-distribution detection. *arXiv preprint arXiv:2306.09301*, 2023c.

Zhang, Y., Lu, J., Peng, B., Fang, Z., and ming Cheung, Y. Learning to shape in-distribution feature space for out-of-distribution detection. In *The Thirty-eighth Annual Conference on Neural Information Processing Systems (NeurIPS)*, 2024.

Zhang, Y., Zhu, W., He, C., and Zhang, L. Lapt: Label-driven automated prompt tuning for ood detection with vision-language models. In Leonardis, A., Ricci, E., Roth, S., Russakovsky, O., Sattler, T., and Varol, G. (eds.), *European Conference on Computer Vision (ECCV)*, pp. 271–288, Cham, 2025. Springer. ISBN 978-3-031-73220-1.

Zhao, Q., Xu, M., Gupta, K., Asthana, A., Zheng, L., and Gould, S. Towards optimal feature-shaping methods for out-of-distribution detection. In *The Twelfth International Conference on Learning Representations (ICLR)*, 2024.

Zhu, J., Geng, Y., Yao, J., Liu, T., Niu, G., Sugiyama, M., and Han, B. Diversified outlier exposure for out-of-distribution detection via informative extrapolation. In Oh, A., Naumann, T., Globerson,

A., Saenko, K., Hardt, M., and Levine, S. (eds.), *Advances in Neural Information Processing Systems (NeurIPS)*, volume 36, pp. 22702–22734, 2023. URL https://proceedings.neurips.cc/paper_files/paper/2023/file/46d943bc6a15a57c923829efc0db7c7a-Paper-Conference.pdf.

Zhu, Y., Chen, Y., Xie, C., Li, X., Zhang, R., Xue, H., Tian, X., Chen, Y., et al. Boosting out-of-distribution detection with typical features. *Advances in Neural Information Processing Systems (NeurIPS)*, 35:20758–20769, 2022.

Zou, Z., Wan, S., Li, G., Han, B., Liu, T., Zhao, L., and Gong, C. Provable discriminative hyperspherical embedding for out-of-distribution detection. In *The AAAI Conference on Artificial Intelligence (AAAI)*, 2025.

Appendix

A. Notations

Table 11 lists all the notations used in this paper.

Table 11. Table of Notations

Notation	Meaning
\mathcal{X}	Input space.
\mathcal{Y}	Label space.
C	Number of classes.
C_{in}	Number of input channels.
h	Classifier.
$\mathcal{P}_{\text{ID}}(x, y)$	Underlying joint distribution of ID data.
$\mathcal{P}_{\text{OOD}}(x)$	Distribution of OOD data.
\mathcal{D}_{ID}	ID training dataset.
N	Number of training samples.
f_{θ}	Feature extractor, parameterized by θ .
\mathcal{A}	Activation space.
$g_{\mathcal{W}}$	Classifier (mapping activations to logits), parameterized by \mathcal{W} .
\mathcal{Z}	Logit space.
\mathbf{a}	Activation vector (output of $f_{\theta}(x)$).
a_j	The j -th element of the activation vector \mathbf{a} .
\mathbf{z}	Logit vector (output of $g_{\mathcal{W}}(\mathbf{a})$).
\mathcal{L}	Loss function (e.g., cross-entropy).
$S(x)$	OOD scoring function.
τ	Threshold for classifying an input as ID or OOD.
x	Input image.
$x[c, h, w]$	Channel value of input image x at position (c, h, w) .
H	Height of the input image.
W	Width of the input image.
$AT(x, c, h, w)$	Attribution function, assigning a score to each channel value of input x .
o	Percent of channel values to perturb.
R	Set of channel value indices with lowest absolute attribution scores.
y_{pred}	Predicted class index.
ε	Perturbation magnitude.
x^{ε}	Perturbed input image.
\mathbf{a}^{ε}	Activation vector of the perturbed input x^{ε} .
$\mathbf{a}^{\text{shift}}$	Activation shift vector (absolute element-wise difference between \mathbf{a} and \mathbf{a}^{ε}).
k_1, k_2	Number of highest-magnitude activations considered for Q and C_o , respectively.
$\text{argsort}(\mathbf{v})$	Same as $\text{argsort}(\mathbf{v})$, $\text{desc} = \text{True}$.
$\text{max}_k(\mathbf{v})$	Returns the indices that would sort the vector \mathbf{v} in descending order.
$\mathbf{i}_1, \mathbf{i}_2$	Returns the k^{th} maximum element of vector \mathbf{v} .
Q	Index sets: $\mathbf{i}_1 = \text{argsort}(\mathbf{a}, \text{desc} = \text{True})[: k_1]$, $\mathbf{i}_2 = \text{argsort}(\mathbf{a}, \text{desc} = \text{True})[: k_2]$
C_o	Sum of activation shifts for the top- k_1 activations.
λ	Correction term: sum of top- k_2 perturbed activations.
Q'	Weighting factor for Q in the Q' calculation.
n_{val}	Estimated OOD likelihood.
\bar{Q}_s	Number of ID validation samples.
$F_{Q'}(Q')$	Set of Q' values on the ID validation samples.
p_{\min}, p_{\max}	Empirical cumulative distribution function (eCDF) of Q' values.
p_r	Minimum and maximum percentile thresholds.
p	Raw ID likelihood from eCDF
$P_p(\mathbf{a})$	Adjusted percentile threshold
r	The p -th percentile value of all elements in \mathbf{a}
$\mathbf{a}_{\text{scaled}}$	Scaling factor.
$\mathbf{z}_{\text{scaled}}$	Scaled activation vector (AdaSCALE-A).
$\text{ReLU}(a_j)$	Scaled logit vector (AdaSCALE-L).
	Rectified Linear Unit activation function: $\text{ReLU}(a_j) = \max(0, a_j)$.

B. Algorithm

The algorithm for computing adaptive scaling factor r is provided in Algorithm 1.

Algorithm 1 Computing the Adaptive Scaling Factor

Input: Input sample x , perturbation magnitude ε , model f_θ , hyperparameters $\lambda, k_1, k_2, p_{\min}, p_{\max}, \varepsilon, o$, precomputed empirical CDF $F_{Q'}$

Output: Scaling factor r

```

1: // Extract features and compute activation shifts
2:  $\mathbf{a} \leftarrow f_\theta(x)$  {Original activation}
3:  $\nabla_x z_c \leftarrow \frac{\partial g_w(f_\theta(x))_c}{\partial x}$  {Gradient for predicted class  $c$ }
4:  $R \leftarrow o\%$  of channel values with lowest  $|\nabla_x z_c|$ 
5:  $x^\varepsilon \leftarrow x + \varepsilon \cdot \text{sign}(\nabla_x z_c) \cdot \mathbb{1}_R$  {Perturb selected regions}
6:  $\mathbf{a}^\varepsilon \leftarrow f_\theta(x^\varepsilon)$  {Perturbed activation}
7:  $\mathbf{a}^{\text{shift}} \leftarrow |\mathbf{a}^\varepsilon - \mathbf{a}|$  {Compute activation shift}
8: // Compute OOD likelihood estimate
9:  $\mathbf{i}_1 \leftarrow \text{argsort}(\mathbf{a}, \text{desc} = \text{True})[: k_1]$ 
10:  $Q \leftarrow \sum_{i \in \mathbf{i}_1} a_i^{\text{shift}}$  {Shift in top activations}
11:  $\mathbf{i}_2 \leftarrow \text{argsort}(\mathbf{a}, \text{desc} = \text{True})[: k_2]$ 
12:  $C_o \leftarrow \sum_{i \in \mathbf{i}_2} \text{ReLU}(a_i^\varepsilon)$  {Correction term}
13:  $Q' \leftarrow \lambda \cdot Q + C_o$  {OOD likelihood estimate}
14: // Compute adaptive percentile
15:  $p_r \leftarrow (1 - F_{Q'}(Q'))$  {raw ID likelihood from eCDF}
16:  $p \leftarrow p_{\min} + p_r \cdot (p_{\max} - p_{\min})$  {Adjusted percentile}
17: // Compute scaling factor
18:  $P_p(\mathbf{a}) \leftarrow$  the  $p$ -th percentile value of all elements in  $\mathbf{a}$ 
19:  $r \leftarrow \sum_j a_j / \sum_{a_j > P_p(\mathbf{a})} a_j$  {Final scaling factor}

```

C. Additional observation in activation space.

Figure 5 shows perturbed activations \mathbf{a}^ε are, on average, higher for ID samples than for OOD samples.

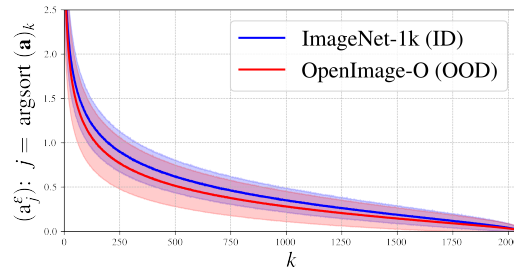


Figure 5. Perturbed activation magnitudes comparison between ID and OOD samples. ID samples consistently maintain higher average activation values in comparison to OOD samples.

D. Additional Experiments and Analysis

D.1. Superiority of the Proposed OODness Metric (Q')

To validate our choice of the OODness metric, we conducted an extensive ablation study comparing the performance of our proposed metric, Q' against Q alone. The results, summarized in Table 12, demonstrate that using Q' provides a consistent and significant performance improvement over using Q alone. This advantage holds across all eight diverse architectures.

Table 12. Comparison of OOD detection performance (FPR95 \downarrow / AUROC \uparrow) using the baseline OODness metric (Q) versus our proposed metric (Q'). The results show a clear advantage for Q' across a wide range of model architectures.

Category	Metric	ResNet-50	ResNet-101	RegNet-Y-16	ResNeXt-50	DenseNet-201	EfficientNetV2-L	ViT-B-16	Swin-B	Average
near-OOD	Q	59.65/77.82	56.67/81.65	60.63/86.00	63.99/79.34	68.65/78.03	73.18/80.17	82.61/69.31	75.85/72.26	68.90/78.07
	Q'	58.98/78.98	57.96/81.68	47.91/89.18	64.14/79.96	61.28/79.66	53.78/86.94	71.87/73.14	73.41/74.48	61.17/80.50
far-OOD	Q	19.82/95.72	20.32/95.50	31.53/93.94	26.87/94.32	35.55/92.19	66.20/84.60	77.52/76.39	63.20/80.78	42.63/89.18
	Q'	17.84/96.14	18.51/95.95	21.37/95.84	22.08/95.24	28.01/93.23	37.61/91.48	47.63/86.83	47.81/87.14	30.11/92.73

For instance, if an OOD sample gets a very high Q score, it will produce a very large scaling factor. This can amplify the logits so much that it washes out the subtle but important information contained within the values of the logits themselves. By adding the opposing term, we "tame" these potentially overconfident scaling factors. This ensures a healthier balance where both the feature-level instability (captured by Q) and the original logit distribution contribute to the final OOD score.

Illustrative Example: A simple toy example demonstrates why this balancing is critical.

Logits: Let $\text{logit}_{\text{ID}} = (1, 6, 2)$ and $\text{logit}_{\text{OOD}} = (1, 1, 1)$.

Case 1: Overconfident Scaling (using only Q)

Let's say this yields scaling factors $r_{\text{ID}} = 2$ and $r_{\text{OOD}} = 5$. Assume a threshold of 25, where energy > 25 is ID and energy < 25 is OOD (We deal with magnitude for simplicity).

$$\text{energy}_{\text{ID}} = \log(e^{1 \cdot 2^2} + e^{6 \cdot 2^2} + e^{2 \cdot 2^2}) = 24.0$$

$$\text{energy}_{\text{OOD}} = \log(e^{1 \cdot 5^2} + e^{1 \cdot 5^2} + e^{1 \cdot 5^2}) = 26.1$$

Here, $\text{energy}_{\text{OOD}} > \text{energy}_{\text{ID}}$, leading to an **OOD detection failure**.

Case 2: Balanced Scaling (using Q' to temper the scaling)

This leads to less extreme scaling, e.g., $r_{\text{ID}} = 1$ and $r_{\text{OOD}} = 2$. Assume a threshold of 5, where energy > 5.5 is ID and energy < 5.5 is OOD (We deal with magnitude for simplicity).

$$\text{energy}_{\text{ID}} = \log(e^{1 \cdot 1^2} + e^{6 \cdot 1^2} + e^{2 \cdot 1^2}) = 6.0$$

$$\text{energy}_{\text{OOD}} = \log(e^{1 \cdot 2^2} + e^{1 \cdot 2^2} + e^{1 \cdot 2^2}) = 5.1$$

Here, $\text{energy}_{\text{ID}} > \text{energy}_{\text{OOD}}$, leading to a **successful OOD detection**.

Table 13. Ablation studies of Q' in FPR@95 \downarrow / AUROC \uparrow format.

Q'	Near-OOD	Far-OOD
Q without scaling	79.81 / 72.32	84.00 / 68.13
Q	59.43 / 78.14	19.70 / 95.73
$\sum_{k=1}^{k_2} \mathbf{a}_{\text{argsort}(\mathbf{a})_k}^{\varepsilon}$	70.39 / 74.00	21.40 / 95.31
$\lambda \cdot Q + \sum_{k=1}^{k_2} \mathbf{a}_{\text{argsort}(\mathbf{a})_k}^{\varepsilon}$	58.97 / 78.98	17.84 / 96.14
$\sum_{k=1}^{k_2} \max_k(\mathbf{a})$	65.11 / 76.23	19.76 / 95.67
$\lambda \cdot Q + \sum_{k=1}^{k_2} \max_k(\mathbf{a})$	58.91 / 78.74	18.02 / 96.08

D.2. Estimated OODness Q' .

Adaptive scaling depends on estimated OODness to determine the extent of scaling. We study the effect of various estimated OODness functions using ResNet-50 network (ImageNet-1k) in Table 13. It clearly shows Q component of Q' being most critical while $\sum_{k=1}^{k_2} \mathbf{a}_{\text{argsort}(\mathbf{a})_k}^{\varepsilon}$ as correction term being a relatively superior choice. However, estimated OODness alone –

without adaptive scaling – does not result in strong performance.

D.3. Comparison with Additional Baselines

Table 14. Comparison with distance-based OOD detection methods on ImageNet-1k using a ResNet-50 backbone. AdaSCALE-A significantly outperforms the distance-based baselines.

Method	Near-OOD		Far-OOD	
	FPR@95 ↓	AUROC ↑	FPR@95 ↓	AUROC ↑
LINe	79.10	67.20	32.95	93.31
NNGuide	72.46	68.09	21.40	95.33
MDS	76.27	64.53	70.82	66.22
AdaSCALE-A	58.97	78.98	17.84	96.14

To situate AdaSCALE within the broader landscape of OOD detection techniques, we compare its performance against additional baselines. The experiments were conducted on the large-scale ImageNet-1k benchmark using a ResNet-50 network. As shown in Table 14, AdaSCALE demonstrates a significant performance advantage over all these methods.

ATS vs AdaSCALE: We provide a more in-depth comparison between ATS and AdaSCALE below:

- **Number of passes:** AdaSCALE uses two forward passes (on the original and perturbed input) to leverage an additional independent OOD detection signal (Q') in its scaling mechanism. In contrast, ATS uses only one forward pass.
- **eCDF Usage:** ATS relies on multiple eCDFs, building one for each selected intermediate layer. AdaSCALE constructs a single eCDF from its final OODness score (Q') in the last layer only. We hypothesize that the final layer is most effective for this, as deeper layers are responsible for semantic discrimination.
- **Role of eCDF:** In ATS, eCDFs are a core part of the inference pipeline, transforming raw activations into p-values that are aggregated to compute the final scaling factor. In AdaSCALE, the single eCDF plays a more indirect, regulatory role: it calibrates the OODness score to determine an adaptive percentile, which then informs the final scaling factor calculation.
- **Data Requirement for eCDF:** AdaSCALE requires only a very small number of ID samples (as few as 5-10). ATS requires access to the whole training dataset to reliably compute eCDFs for each intermediate layer.

D.4. Analysis on Adversarially Trained Models

We investigate the effectiveness of our approach on adversarially trained models to test its robustness. This analysis is twofold: first, we verify that the core assumption of our method holds, and second, we evaluate its OOD detection performance.

D.4.1. ACTIVATION SENSITIVITY IN ADVERSARILY TRAINED NETWORKS

The effectiveness of our method relies on the activation shift ratio (Q_{OOD}/Q_{ID}) being greater than 1 for OOD samples compared to ID samples. We measured this ratio by taking the top-1% activation shifts on a ResNet-50 model adversarially trained on ImageNet-1k. The results in Table 15 confirm that the ratio remains consistently greater than 1 across various OOD datasets. This demonstrates that OOD samples still produce a larger activation shift than ID samples, even in adversarially robust models, validating our method’s applicability.

D.4.2. PERFORMANCE OF ADASCALE ON ADVERSARILY TRAINED NETWORKS

We evaluate AdaSCALE’s OOD detection performance on these adversarially trained models using the exact same hyperparameters as for the standard ResNet-50. The results in Table 16 show that AdaSCALE consistently outperforms baseline methods. This highlights the robustness of our approach AdaSCALE, which remains superior even when applied to models with different training schemes without any specific hyperparameter tuning.

Table 15. Activation shift ratio (Q_{OOD}/Q_{ID}) on a ResNet-50 model adversarially trained on ImageNet-1k. The ratio remaining greater than 1 confirms that the fundamental signal required for our method persists.

OOD Dataset	Q_{OOD}/Q_{ID} ($\epsilon = 0.01$)	Q_{OOD}/Q_{ID} ($\epsilon = 0.05$)
SSB-hard	1.78	1.73
NINCO	1.29	1.28
ImageNet-O	1.69	1.72
OpenImage-O	1.48	1.45
iNaturalist	1.14	1.14
Textures	1.33	1.18
Places	1.30	1.16

Table 16. OOD detection performance on adversarially trained ResNet-50 models. AdaSCALE consistently outperforms the baselines, demonstrating its robustness.

Training	Method	Near-OOD		Far-OOD	
		FPR@95 ↓	AUROC ↑	FPR@95 ↓	AUROC ↑
$\epsilon = 0.01$	SCALE	68.54	75.43	25.95	94.40
	OptFS	70.36	72.97	28.60	93.24
	AdaSCALE-A	60.73	80.84	19.90	95.74
$\epsilon = 0.05$	SCALE	66.99	76.10	24.77	94.40
	OptFS	70.11	73.51	28.32	93.42
	AdaSCALE-A	60.21	80.68	21.13	95.35

D.5. Robustness to Real-World Image Corruptions

To evaluate the practical robustness of our method, we assess its performance when input images are subjected to common real-world corruptions. We benchmark AdaSCALE against SCALE and OptFS on the ImageNet-1k dataset using a ResNet-50, applying Gaussian blur and JPEG compression to the input images. The results, presented without any hyperparameter re-tuning, show that AdaSCALE’s performance advantage is maintained even under these challenging conditions.

Table 17. OOD detection performance with Gaussian blur (kernel size=5, sigma=(0.1, 2.0)).

Method	Near-OOD		Far-OOD	
	FPR@95 ↓	AUROC ↑	FPR@95 ↓	AUROC ↑
SCALE	72.68	70.15	29.65	92.72
OptFS	71.84	69.66	30.27	92.24
AdaSCALE-A	67.53	75.18	28.11	93.31

Table 18. OOD detection performance with 50% JPEG compression.

Method	Near-OOD		Far-OOD	
	FPR@95 ↓	AUROC ↑	FPR@95 ↓	AUROC ↑
SCALE	69.73	71.84	27.46	93.56
OptFS	69.43	71.12	28.34	92.95
AdaSCALE-A	61.24	77.59	25.87	94.06

E. Sensitivity study with ViT-B-16 model

Table 19. Sensitivity study of individual hyperparameters for ViT-B-16. Results are reported as FPR@95 (↓) / AUROC (↑).

Parameter	Value	Near-OOD	Far-OOD
ϵ			
0.1		72.71 / 73.06	46.60 / 87.22
0.5		71.87 / 73.14	47.63 / 86.83
1.0		72.92 / 73.06	49.80 / 86.49
λ			
1		73.92 / 72.22	47.15 / 87.15
10		71.87 / 73.14	47.63 / 86.83
20		72.94 / 73.22	51.96 / 85.93
30		73.72 / 73.06	54.55 / 84.16
k_1			
1		71.87 / 73.14	47.63 / 86.83
2		72.47 / 73.37	51.60 / 85.96
3		73.20 / 73.10	54.79 / 85.12
k_2			
5		71.87 / 73.14	47.63 / 86.83
10		72.06 / 73.26	47.55 / 87.03
20		72.58 / 72.87	47.89 / 86.96
o			
2		72.28 / 73.65	47.70 / 87.02
5		71.87 / 73.14	47.63 / 86.83
10		72.34 / 73.30	48.86 / 86.69
p_{max}			
75		76.87 / 71.78	52.97 / 86.07
80		72.60 / 73.24	48.57 / 86.78
85		71.87 / 73.14	47.63 / 86.83
90		72.40 / 73.65	48.80 / 86.64
95		72.35 / 73.63	48.73 / 86.69

Table 20. Joint sensitivity study of 4 hyperparameters in ViT-B-16. The metric reported is Validation AUROC.

ϵ	λ	σ	p_{\max}	Val AUROC
0.1	1	2	80	87.13
			85	87.55
			90	87.74
	10	5	80	87.11
			85	87.53
			90	87.73
	20	2	80	87.07
			85	87.47
			90	87.65
	0.5	5	80	87.46
			85	87.74
			90	87.78
	10	10	80	87.43
			85	87.71
			90	87.77
	20	10	80	87.41
			85	87.72
			90	87.79
	1	2	80	87.59
			85	87.77
			90	87.67
	10	20	80	87.54
			85	87.73
			90	87.63
	0.5	10	80	87.48
			85	87.68
			90	87.62
	20	10	80	87.08
			85	87.47
			90	87.65
	1	5	80	86.94
			85	87.29
			90	87.41
	10	20	80	86.65
			85	86.87
			90	86.88
	0.5	10	80	87.16
			85	87.47
			90	87.54
	20	5	80	86.92
			85	87.25
			90	87.35
	1	10	80	86.76
			85	87.15
			90	87.32
	10	20	80	86.86
			85	86.98
			90	86.86
	0.5	20	80	86.40
			85	86.58
			90	86.53
	1	10	80	86.09
			85	86.43
			90	86.55
	10	5	80	87.00
			85	87.34
			90	87.45
	20	1	80	86.72
			85	86.90
			90	86.87
	1	10	80	85.96
			85	85.81
			90	85.42
	10	2	80	86.73
			85	87.09
			90	87.22
	20	10	80	86.31
			85	86.71
			90	86.93
	1	20	80	85.97
			85	86.42
			90	86.69
	10	2	80	86.00
			85	86.23
			90	86.23
	20	10	80	85.27
			85	85.60
			90	85.75
	1	20	80	84.69
			85	85.09
			90	85.35

F. Sensitivity study with ResNet-50 model

F.1. Sensitivity study of ε

The sensitivity study of ε presented at Table 21 suggests the optimal value of ε to be around 0.5.

Table 21. Sensitivity study of ε with ResNet-50 model on ImageNet-1k benchmark.

ε	Near-OOD		Far-OOD	
	FPR@95 ↓	AUROC ↑	FPR@95 ↓	AUROC ↑
0.1	63.76	77.50	19.26	95.85
0.5	58.97	78.98	17.84	96.14
1.0	61.60	76.96	19.31	95.84

F.2. Sensitivity study of λ

The sensitivity study of λ presented at Table 21 suggests the optimal value of λ to be around 10.

Table 22. Sensitivity study of λ with ResNet-50 model on ImageNet-1k benchmark.

λ	Near-OOD		Far-OOD	
	FPR@95 ↓	AUROC ↑	FPR@95 ↓	AUROC ↑
0.1	70.07	74.12	21.40	95.33
1	67.49	75.45	20.41	95.54
10	58.97	78.98	17.84	96.14
100	59.03	78.10	19.39	95.80

F.3. Sensitivity study of k_1

The sensitivity study of k_1 presented at Table 23 suggests the optimal value of k_1 to be around 1%.

Table 23. Sensitivity study of k_1 with ResNet-50 model on ImageNet-1k benchmark.

k_1	Near-OOD		Far-OOD	
	FPR@95 ↓	AUROC ↑	FPR@95 ↓	AUROC ↑
1%	58.97	78.98	17.84	96.14
5%	60.36	77.74	19.95	95.63
10%	60.40	77.89	19.72	95.63
50%	60.34	77.25	20.90	95.25
100%	60.99	76.49	21.88	94.96

F.4. Sensitivity study of k_2

The sensitivity study of k_2 presented at Table 24 suggests the optimal value of k_2 to be around 5%.

F.5. Sensitivity study of o

We present the complete results of image perturbation study (FPR@95 ↓ / AUROC ↑) in Table 25.

Table 24. Sensitivity study of k_2 with ResNet-50 model on ImageNet-1k benchmark.

k_2	Near-OOD		Far-OOD	
	FPR@95 \downarrow	AUROC \uparrow	FPR@95 \downarrow	AUROC \uparrow
1%	59.08	78.56	18.35	96.02
5%	58.97	78.98	17.84	96.14
10%	59.41	78.65	18.33	95.96
100%	62.43	75.44	23.05	94.69

Table 25. Image perturbation study with ResNet-50 model on ImageNet-1k benchmark.

Pixel type	$o\%$	OOD Detection		FS-OOD Detection	
		Near-OOD	Far-OOD	Near-OOD	Far-OOD
Random	1%	61.73 / 78.15	19.44 / 95.74	83.19 / 48.59	53.45 / 74.10
	5%	59.97 / 78.67	18.14 / 96.06	81.92 / 49.19	52.35 / 74.84
	10%	60.27 / 78.02	18.45 / 96.00	82.07 / 48.62	52.84 / 74.70
	50%	62.81 / 76.27	19.95 / 95.70	83.40 / 46.55	54.94 / 73.42
Trivial	1%	61.77 / 78.29	19.28 / 95.77	82.92 / 48.86	53.34 / 74.24
	5%	58.97 / 78.98	17.84 / 96.14	81.52 / 49.35	52.33 / 74.89
	10%	60.24 / 78.17	17.94 / 96.08	82.19 / 48.59	52.59 / 74.77
	50%	66.43 / 74.10	21.58 / 95.29	85.26 / 44.86	56.56 / 72.82
Salient	1%	69.43 / 75.13	22.62 / 95.17	85.59 / 48.32	53.76 / 75.23
	5%	67.31 / 75.78	21.24 / 95.44	85.07 / 48.40	53.26 / 75.63
	10%	65.65 / 76.20	20.39 / 95.62	84.36 / 48.33	53.17 / 75.55
	50%	64.54 / 75.39	20.48 / 95.61	83.78 / 47.07	54.11 / 74.54
All	100%	67.37 / 73.08	22.93 / 95.01	85.66 / 44.00	57.80 / 72.19

F.6. Sensitivity study of p_{\min}

We present sensitivity study (FPR@95 \downarrow / AUROC \uparrow) of p_{\min} , setting p_{\max} to 85 in the Table 26.

 Table 26. Sensitivity study of p_{\min} with ResNet-50 model on ImageNet-1k benchmark.

p_{\min}	70	75	80	85
Near-OOD	62.54 / 79.60	58.57 / 81.68	58.98 / 78.98	67.76 / 74.20
Far-OOD	21.62 / 95.19	19.86 / 95.62	17.84 / 96.14	21.44 / 95.39

F.7. Joint sensitivity study

We present joint sensitivity study in terms of near-OOD detection among three hyperparameters ($\lambda, p_{\max}, p_{\min}$) below:

The results in Table 27 clearly indicate that the λ hyperparameter exerts a more significant influence on the final OOD detection performance. Furthermore, a key relationship emerges: for optimal performance, a decrease in λ must be compensated by an increase in Q (and consequently, a higher k_1). This is explained by the formulation $Q' = \lambda \cdot Q + C_o$, where a smaller λ necessitates a larger Q value to ensure the term $\lambda \cdot Q$ dominates the regularizer C_o .

In Table 28, when λ is set to 0.1 with $k_1 = 1\%$, $\lambda \cdot Q$ does not dominate over C_o term. As a result, it leads to scaling based on the regularization / balancing term instead of "predetermined" actual OOD detection signal "activation shift at peak activations". Such value of λ (e.g., $\lambda = 0.1$) invalidates the proposed hypothesis.

From the results in Table 29, it can be observed that activation shift with all activations considered ($k_1 = 100\%$) still proves to be a useful OOD detection signal.

Table 27. Joint sensitivity study of k_1 and λ (setting $p_{\max} = 85\%$) with ResNet-50 model on ImageNet-1k benchmark.

$k_1 \setminus \lambda$	0.1	1	10	100
1%	70.07 / 74.12	67.49 / 75.45	58.97 / 78.98	59.03 / 78.10
5%	69.53 / 74.33	63.87 / 76.84	60.36 / 77.74	61.12 / 77.22
10%	69.34 / 74.50	62.63 / 77.33	60.40 / 77.89	61.55 / 76.92
50%	67.49 / 75.32	61.26 / 77.26	60.34 / 77.25	62.05 / 76.52
100%	65.95 / 75.77	61.18 / 76.97	62.17 / 76.39	62.43 / 76.31

 Table 28. Joint sensitivity study of λ and p_{\max} (setting $k_1 = 1\%$) with ResNet-50 model on ImageNet-1k benchmark.

$\lambda \setminus p_{\max}$	85	90	95
0.1	70.07 / 74.12	87.45 / 66.06	91.81 / 56.09
1	67.49 / 75.45	84.31 / 69.32	89.41 / 60.11
10	58.97 / 78.98	69.47 / 79.68	78.77 / 76.26
100	59.03 / 78.10	63.19 / 79.67	71.43 / 78.51

Furthermore, previous works (ASH, SCALE) observed that, particularly for ResNet-50 architecture, the performance drops after the percentile value of 85%. Similar observations can also be made in AdaSCALE from the results in Tables 28 and 29.

 Table 29. Joint sensitivity study of k_1 and p_{\max} (setting $\lambda = 10$) with ResNet-50 model on ImageNet-1k benchmark.

$k_1 \setminus p_{\max}$	85	90	95
1%	58.97 / 78.98	69.49 / 79.67	78.77 / 76.26
5%	60.36 / 77.74	68.30 / 78.23	78.19 / 75.58
10%	60.40 / 77.89	68.46 / 77.46	78.90 / 74.70
50%	60.34 / 77.25	69.88 / 76.39	80.46 / 73.17
100%	62.17 / 76.39	70.13 / 75.93	81.22 / 72.32

G. ISH regularization:

Apart from enhancing the prior postprocessor ASH (Djurisic et al., 2023), SCALE (Xu et al., 2015) introduces a training regularization to emphasize samples with more distinct ID characteristics. We assess the performance (FPR@95 ↓ / AUROC ↑) of each method in ResNet-50 and ResNet-101 model following this regularization in Table 30. The results indicate that AdaSCALE maintains a substantial advantage, surpassing the second-best method, SCALE, by **12.56% / 5.82%** and **20.46% / 1.21%** in FPR@95 / AUROC for near- and far-OOD detection in ResNet-50, respectively. Moreover, AdaSCALE demonstrates superior performance beyond conventional OOD detection, with corresponding improvements of **4.10% / 5.87%** and **9.70% / 1.12%** in full-spectrum setting. Furthermore, ISH regularization further amplifies the performance gap between AdaSCALE-A and OptFS, enhancing the near-OOD detection improvement from 12.96% / 6.44% to **15.18% / 14.83%**. These findings also generalize to ResNet-101 network.

Table 30. OOD detection results on ImageNet-1k benchmark with ISH (Xu et al., 2024) regularization.

Method	OOD Detection		FS-OOD Detection	
	Near-OOD	Far-OOD	Near-OOD	Far-OOD
ResNet-50				
MSP	74.07 / 62.16	51.13 / 84.64	87.52 / 40.36	74.41 / 61.52
MLS	74.38 / 66.43	41.57 / 88.90	88.89 / 39.49	71.53 / 61.69
EBO	74.68 / 66.46	41.85 / 88.83	89.05 / 39.18	71.77 / 61.11
ReAct	71.98 / 70.81	28.76 / 93.49	87.78 / 43.88	61.87 / 71.64
ASH	67.99 / 73.46	23.88 / 94.67	85.74 / 45.29	57.81 / 72.81
SCALE	65.68 / 76.41	20.77 / 95.62	84.31 / 48.40	54.48 / 74.79
BFAct	71.59 / 70.85	28.38 / 93.50	87.51 / 43.95	61.39 / 71.43
LTS	66.32 / 75.03	22.07 / 95.28	85.08 / 46.16	57.11 / 73.06
OptFS	67.71 / 73.03	24.65 / 94.18	85.38 / 45.91	57.09 / 72.95
AdaSCALE-A	57.43 / 80.86	16.52 / 96.46	80.85 / 51.24	51.57 / 75.63
AdaSCALE-L	56.83 / 80.81	17.62 / 96.22	80.97 / 50.59	53.43 / 74.62
ResNet-101				
MSP	71.39 / 68.31	51.00 / 84.81	85.70 / 45.72	73.69 / 62.79
MLS	72.32 / 71.94	41.04 / 88.99	87.39 / 44.88	69.94 / 63.23
EBO	72.78 / 71.92	41.45 / 88.87	87.64 / 44.66	70.23 / 62.65
ReAct	67.74 / 75.74	28.53 / 93.47	85.40 / 48.83	60.50 / 72.18
ASH	66.03 / 77.79	25.21 / 94.43	83.95 / 50.57	56.91 / 73.37
SCALE	64.30 / 78.98	23.09 / 94.95	83.14 / 51.05	55.88 / 73.27
BFAct	67.53 / 75.86	28.32 / 93.40	85.11 / 48.96	60.12 / 71.83
LTS	66.32 / 75.03	22.07 / 95.28	85.08 / 46.16	57.11 / 73.06
OptFS	67.71 / 73.03	24.65 / 94.18	85.38 / 45.91	57.09 / 72.95
AdaSCALE-A	54.66 / 83.52	16.81 / 96.32	78.52 / 55.19	49.92 / 76.20
AdaSCALE-L	53.91 / 83.49	17.55 / 96.15	78.63 / 54.60	51.47 / 75.47

H. Hyperparameters

We present final hyperparameter values of AdaSCALE-A and AdaSCALE-L in Table 31 and Table 32.

Table 31. Hyperparameters (p_{\min} , p_{\max}) used for each dataset and network for AdaSCALE-A.

Dataset	Network	p_{\min}	p_{\max}
CIFAR-10	WideResNet-28-10	60	95
	DenseNet-101	65	90
CIFAR-100	WideResNet-28-10	60	85
	DenseNet-101	70	80
ImageNet-1k	ResNet-50	80	85
	ResNet-101	80	85
	RegNet-Y-16	60	90
	ResNeXt-50	80	85
	DenseNet-201	90	95
	EfficientNetV2-L	60	99
	Vit-B-16	60	85
	Swin-B	90	99

Table 32. Hyperparameters (p_{\max} , p_{\min}) used for each dataset and network for AdaSCALE-L.

Dataset	Network	p_{\min}	p_{\max}
CIFAR-10	WideResNet-28-10	60	85
	DenseNet-101	70	85
CIFAR-100	WideResNet-28-10	60	80
	DenseNet-101	65	75
ImageNet-1k	ResNet-50	80	85
	ResNet-101	70	80
	RegNet-Y-16	60	85
	ResNeXt-50	70	80
	DenseNet-201	90	95
	EfficientNetV2-L	60	99
	Vit-B-16	75	85
	Swin-B	90	99

I. CIFAR-results

I.1. WRN-28-10

Table 33. Far-OOD detection results (FPR@95 \downarrow / AUROC \uparrow) on CIFAR-10 and CIFAR-100 benchmarks using the WRN-28-10 network, averaged over 3 trials. The overall average performance is reported. The best results are **bold**, and the second-best results are underlined.

Method	CIFAR-10 benchmark				
	MNIST	SVHN	Textures	Places365	Average
MSP	17.02 / 94.61	21.71 / 92.96	60.50 / 88.06	42.27 / 90.04	35.38 / 91.42
MLS	<u>13.01</u> / <u>96.76</u>	30.35 / 93.06	76.12 / 86.65	52.56 / 90.46	43.01 / 91.73
EBO	12.93 / 96.93	30.35 / 93.12	76.15 / 86.68	52.57 / 90.56	43.00 / 91.82
ReAct	15.50 / 96.30	34.01 / 92.47	<u>57.76</u> / 88.77	57.33 / 89.66	41.15 / 91.80
ASH	50.11 / 88.80	89.90 / 74.76	95.07 / 72.91	92.22 / 70.06	81.82 / 76.63
SCALE	13.24 / 96.70	32.21 / 92.88	75.76 / 86.77	55.81 / 90.09	44.26 / 91.61
BFAct	25.79 / 94.64	43.08 / 91.10	57.16 / 88.80	61.00 / 88.32	46.75 / 90.71
LTS	14.04 / 96.60	39.85 / 92.21	76.85 / 86.43	63.13 / 89.19	48.47 / 91.11
OptFS	25.68 / 94.83	51.58 / 89.86	62.14 / 88.07	80.19 / 84.05	54.90 / 89.20
AdaSCALE-A	14.93 / 96.02	17.84 / 95.14	64.96 / 88.31	34.57 / 92.31	33.08 / 92.95
AdaSCALE-L	15.58 / 95.98	<u>18.41</u> / <u>95.10</u>	62.87 / 88.67	<u>37.59</u> / <u>91.97</u>	<u>33.61</u> / <u>92.93</u>

Method	CIFAR-100 benchmark				
	MNIST	SVHN	Textures	Places365	Average
MSP	49.79 / 78.72	56.76 / 80.70	64.49 / 76.86	<u>56.66</u> / 79.96	56.92 / 79.06
MLS	46.57 / 81.43	53.08 / 83.37	64.59 / 77.65	59.70 / 79.82	55.99 / 80.57
EBO	46.41 / 81.99	52.92 / 83.77	64.58 / 77.61	59.76 / 79.60	55.92 / 80.74
ReAct	49.92 / 81.07	40.66 / 86.49	52.42 / 80.81	60.35 / 79.72	50.84 / 82.03
ASH	<u>44.06</u> / <u>85.55</u>	41.48 / 87.50	61.78 / 81.65	80.45 / 71.83	56.94 / 81.63
SCALE	<u>40.65</u> / 84.68	48.56 / 85.56	58.45 / 80.81	60.51 / 79.90	52.04 / 82.74
BFAct	61.59 / 77.47	34.74 / 88.50	47.30 / <u>83.38</u>	64.49 / 78.47	52.03 / 81.96
LTS	36.27 / 87.38	45.41 / 87.23	53.90 / 83.18	62.62 / 79.64	<u>49.55</u> / <u>84.36</u>
OptFS	57.61 / 79.47	37.04 / 86.43	53.02 / 80.43	70.44 / 76.77	54.53 / 80.78
AdaSCALE-A	45.18 / 81.69	<u>36.79</u> / 89.20	55.93 / 81.93	56.48 / 81.55	48.59 / 83.59
AdaSCALE-L	42.13 / 83.58	32.44 / 91.02	<u>50.87</u> / 84.14	57.83 / <u>81.51</u>	45.82 / 85.06

Table 34. Near-OOD detection results (FPR@95 \downarrow / AUROC \uparrow) on CIFAR-10 and CIFAR-100 benchmarks using the WRN-28-10 network, averaged over 3 trials. The overall average performance is reported. The best results are **bold**, and the second-best results are underlined.

Method	CIFAR-10 benchmark		CIFAR-100 benchmark		Average
	CIFAR-100	TIN	CIFAR-10	TIN	
MSP	54.13 / 88.28	<u>42.94</u> / 89.93	56.83 / 80.42	48.82 / 83.39	<u>50.68</u> / 85.51
MLS	67.10 / 87.72	55.91 / 89.90	<u>58.99</u> / 80.98	49.27 / 84.01	57.82 / 85.65
EBO	67.04 / 87.77	55.88 / 89.97	<u>58.97</u> / <u>80.93</u>	49.39 / 83.95	57.82 / 85.66
ReAct	65.96 / 87.76	51.44 / 90.33	69.17 / 79.10	51.56 / 83.77	59.53 / 85.24
ASH	91.33 / 70.72	90.77 / 73.28	85.25 / 69.96	78.31 / 74.55	86.42 / 72.13
SCALE	69.52 / 87.35	59.48 / 89.53	61.30 / 80.35	51.25 / 83.65	60.39 / 85.22
BFAct	66.31 / 86.94	57.12 / 89.69	78.90 / 74.98	59.04 / 82.25	65.34 / 83.47
LTS	74.28 / 86.38	66.01 / 88.56	64.17 / 79.57	54.24 / 83.09	64.68 / 84.40
OptFS	76.36 / 84.05	66.73 / 86.56	85.40 / 75.55	64.11 / 80.99	73.15 / 79.83
AdaSCALE-A	50.60 / 89.40	42.80 / 91.13	62.21 / 79.99	47.11 / 84.98	50.68 / 86.38
AdaSCALE-L	<u>53.98</u> / <u>89.01</u>	45.95 / <u>90.77</u>	65.41 / 79.27	<u>48.74</u> / <u>84.75</u>	53.52 / <u>85.95</u>

I.2. DenseNet-101

Table 35. Far-OOD detection results (FPR@95 \downarrow / AUROC \uparrow) on CIFAR-10 and CIFAR-100 benchmarks using the DenseNet-101 network, averaged over 3 trials. The overall average performance is reported. The best results are **bold**, and the second-best results are underlined.

Method	CIFAR-10 benchmark					Average
	MNIST	SVHN	Textures	Places365		
MSP	17.91 / 94.22	32.04 / 90.38	46.80 / 87.53	37.59 / 89.24	33.59 / 90.34	
MLS	10.02 / 97.58	31.25 / 92.59	64.43 / 85.58	39.19 / 90.74	36.22 / 91.62	
EBO	9.74 / 97.76	31.23 / 92.69	64.46 / 85.48	39.17 / 90.81	36.15 / 91.68	
ReAct	12.60 / 97.24	34.79 / 92.02	<u>50.41</u> / 88.21	36.12 / 91.35	33.48 / 92.20	
ASH	9.40 / 98.12	39.42 / 91.25	70.95 / 85.39	57.90 / 85.48	44.42 / 90.06	
SCALE	<u>9.04</u> / 97.88	26.99 / 93.54	61.52 / 86.77	39.57 / 90.76	34.28 / 92.24	
BFAct	23.59 / 94.96	42.49 / 89.00	53.74 / 87.38	37.53 / 91.09	39.34 / 90.61	
LTS	8.92 / <u>97.97</u>	27.16 / 93.59	59.07 / 87.09	39.47 / 90.81	33.65 / <u>92.37</u>	
OptFS	9.74 / 97.88	41.20 / 90.71	51.35 / 88.48	59.47 / 86.03	40.44 / 90.77	
AdaSCALE-A	12.42 / 96.85	25.04 / 94.05	58.28 / 87.35	<u>36.77</u> / <u>91.20</u>	33.13 / 92.36	
AdaSCALE-L	10.92 / 97.44	<u>26.43</u> / <u>93.87</u>	58.59 / 87.19	37.03 / 91.25	<u>33.24</u> / 92.44	
CIFAR-100 benchmark						
MSP	65.65 / 72.43	63.81 / 76.52	75.34 / 72.19	<u>61.36</u> / 77.16	66.54 / 74.57	
MLS	58.69 / 78.55	57.12 / 79.43	79.05 / 72.68	62.72 / 78.38	64.39 / 77.26	
EBO	58.58 / 78.98	<u>56.76</u> / 79.19	79.09 / 72.44	62.86 / 78.08	64.32 / 77.17	
ReAct	62.71 / 76.37	48.48 / 81.64	64.65 / 78.62	59.00 / 78.89	<u>58.71</u> / 78.88	
ASH	40.69 / 88.57	48.03 / 86.24	<u>65.24</u> / 83.29	73.29 / 71.88	56.81 / 82.49	
SCALE	56.92 / 79.53	53.81 / 80.96	76.10 / 74.47	62.49 / 78.51	62.33 / 78.37	
BFAct	73.83 / 67.19	60.01 / 75.85	69.29 / 76.41	68.15 / 73.73	67.82 / 73.29	
LTS	<u>55.33</u> / <u>80.58</u>	51.33 / 82.04	73.06 / 75.89	62.58 / 78.36	60.58 / 79.22	
OptFS	64.24 / 75.24	59.81 / 76.46	66.15 / 77.50	73.47 / 69.76	65.92 / 74.74	
AdaSCALE-A	62.51 / 74.96	<u>46.29</u> / 84.31	71.40 / 76.59	61.70 / <u>78.86</u>	60.47 / 78.68	
AdaSCALE-L	61.33 / 75.73	43.97 / <u>85.30</u>	69.31 / 77.71	61.97 / 78.69	59.15 / <u>79.36</u>	

Table 36. Near-OOD detection results (FPR@95 \downarrow / AUROC \uparrow) on CIFAR-10 and CIFAR-100 benchmarks using the DenseNet-101 network, averaged over 3 trials. The overall average performance is reported. The best results are **bold**, and the second-best results are underlined.

Method	CIFAR-10 benchmark		CIFAR-100 benchmark		Average
	CIFAR-100	TIN	CIFAR-10	TIN	
MSP	40.13 / 88.45	35.50 / 89.61	59.94 / 77.53	56.96 / 79.57	48.13 / 83.79
MLS	45.14 / 88.85	38.01 / 90.85	<u>63.61</u> / 78.26	57.09 / 81.75	50.96 / 84.93
EBO	45.19 / 88.85	38.05 / 90.90	63.90 / 77.94	57.53 / 81.58	51.17 / 84.82
ReAct	44.34 / 89.19	37.10 / 91.08	70.77 / 75.06	61.30 / 80.40	53.38 / 83.93
ASH	67.78 / 82.68	62.54 / 85.18	81.65 / 65.84	78.66 / 70.01	72.66 / 75.93
SCALE	45.25 / 88.92	37.76 / 91.01	64.20 / <u>78.13</u>	56.96 / 81.88	51.04 / 84.99
BFAct	52.06 / 87.70	44.09 / 89.89	79.31 / 67.39	71.79 / 74.18	61.81 / 79.79
LTS	44.89 / 89.03	37.67 / 91.10	64.66 / 77.87	56.83 / 81.87	51.01 / 84.97
OptFS	60.63 / 85.29	55.55 / 86.96	82.97 / 64.99	74.73 / 70.55	68.47 / 76.95
AdaSCALE-A	43.29 / 89.37	<u>35.57</u> / <u>91.32</u>	65.51 / 78.00	54.49 / <u>82.44</u>	<u>49.72</u> / 85.28
AdaSCALE-L	<u>43.19</u> / 89.40	35.70 / 91.37	66.09 / 77.79	<u>54.57</u> / 82.47	49.89 / <u>85.26</u>

J. ImageNet-1k results

J.1. near-OOD detection

Table 37. Near-OOD detection results (FPR@95 \downarrow / AUROC \uparrow) on ImageNet-1k benchmark using ResNet-50 network. The best results are **bold**, and the second-best results are underlined.

Method	SSB-Hard	NINCO	ImageNet-O	Average
MSP	74.49 / 72.09	56.88 / 79.95	91.32 / 28.60	74.23 / 60.21
MLS	76.20 / 72.51	59.44 / 80.41	88.97 / 40.73	74.87 / 64.55
EBO	76.54 / 72.08	60.58 / 79.70	88.84 / 41.78	75.32 / 64.52
REACT	77.55 / 73.03	55.82 / 81.73	84.45 / 51.67	72.61 / 68.81
ASH	73.66 / 72.89	53.05 / 83.45	81.70 / 57.67	69.47 / 71.33
SCALE	67.72 / 77.35	51.80 / 85.37	83.77 / 59.89	67.76 / 74.20
BFAct	77.20 / 73.15	55.27 / 81.88	84.57 / 51.62	72.35 / 68.88
LTS	68.46 / 77.10	51.24 / 85.33	84.33 / 57.69	68.01 / 73.37
OptFS	78.32 / 71.01	52.09 / 82.51	78.56 / 59.40	69.66 / 70.97
AdaSCALE-A	57.96 / 81.68	44.92 / 87.15	74.06 / 68.12	58.98 / 78.98
AdaSCALE-L	<u>58.68 / 81.42</u>	<u>45.01 / 87.11</u>	<u>75.83 / 67.33</u>	<u>59.84 / 78.62</u>

Table 38. Near-OOD detection results (FPR@95 \downarrow / AUROC \uparrow) on ImageNet-1k benchmark using ResNet-101 network. The best results are **bold**, and the second-best results are underlined.

Method	SSB-Hard	NINCO	ImageNet-O	Average
MSP	73.20 / 72.57	55.27 / 80.61	87.42 / 48.57	71.96 / 67.25
MLS	74.68 / 74.37	55.65 / 82.29	85.81 / 57.89	72.05 / 71.51
EBO	74.96 / 74.12	56.33 / 81.79	85.66 / 58.72	72.32 / 71.54
REACT	75.96 / 74.43	52.58 / 83.27	75.67 / 67.31	68.07 / 75.00
ASH	72.48 / 74.23	49.41 / 84.62	73.84 / 70.98	65.24 / 76.61
SCALE	68.47 / 77.10	49.03 / 86.20	74.09 / 72.50	63.87 / 78.60
BFAct	75.48 / 74.74	52.23 / 83.37	76.16 / 67.37	67.96 / 75.16
OptFS	76.55 / 72.29	50.89 / 83.35	68.94 / 71.85	65.46 / 75.83
AdaSCALE-A	61.00 / 80.29	46.70 / 86.99	62.05 / 78.27	56.59 / 81.85
AdaSCALE-L	<u>61.05 / 80.41</u>	<u>47.77 / 86.84</u>	<u>60.40 / 78.35</u>	<u>56.41 / 81.86</u>

Table 39. Near-OOD detection results (FPR@95 \downarrow / AUROC \uparrow) on ImageNet-1k benchmark using RegNet-Y-16 network. The best results are **bold**, and the second-best results are underlined.

Method	SSB-Hard	NINCO	ImageNet-O	Average
MSP	65.35 / 78.28	48.48 / 86.85	72.82 / 77.09	62.22 / 80.74
MLS	62.48 / 84.83	42.76 / 91.56	83.60 / 77.58	62.94 / 84.66
EBO	<u>62.10</u> / <u>85.28</u>	<u>42.49</u> / <u>91.67</u>	83.82 / 77.33	62.80 / 84.76
REACT	73.02 / 73.17	59.81 / 80.91	79.37 / 72.02	70.73 / 75.37
ASH	80.58 / 67.70	77.23 / 71.42	89.71 / 64.30	82.51 / 67.81
SCALE	66.98 / 82.35	49.84 / 89.93	84.44 / 76.43	67.09 / 82.90
BFAct	79.40 / 64.39	73.98 / 70.35	82.76 / 63.54	78.72 / 66.09
LTS	69.52 / 79.78	55.38 / 87.71	84.55 / 74.78	69.82 / 80.75
OptFS	79.59 / 69.47	63.97 / 80.36	77.03 / 75.79	73.53 / 75.21
AdaSCALE-A	54.50 / 87.21	31.50 / 93.50	57.75 / 86.83	47.91 / 89.18
AdaSCALE-L	62.61 / 84.60	47.84 / 90.13	<u>57.94</u> / <u>86.61</u>	<u>56.13</u> / <u>87.11</u>

Table 40. Near-OOD detection results (FPR@95 \downarrow / AUROC \uparrow) on ImageNet-1k benchmark using ResNeXt-50 network. The best results are **bold**, and the second-best results are underlined.

Method	SSB-Hard	NINCO	ImageNet-O	Average
MSP	73.04 / 73.28	57.90 / 80.86	88.81 / 49.43	73.25 / 67.86
MLS	74.68 / 75.06	60.79 / 81.91	86.87 / 57.87	74.11 / 71.61
EBO	74.90 / 74.89	60.96 / 81.44	86.76 / 58.49	74.21 / 71.61
REACT	75.54 / 74.51	57.29 / 82.50	80.03 / 65.37	70.95 / 74.13
ASH	70.72 / 76.64	58.40 / 83.49	83.84 / 65.63	70.99 / 75.25
SCALE	67.77 / 79.73	56.87 / 85.39	87.15 / 63.48	70.60 / 76.20
BFAct	75.36 / 74.65	57.65 / 82.46	79.86 / 65.30	70.96 / 74.14
LTS	68.26 / 79.36	56.35 / 85.39	86.22 / 63.85	70.28 / 76.20
OptFS	75.62 / 73.82	57.07 / 82.37	75.13 / 68.33	69.27 / 74.84
AdaSCALE-A	61.03 / 81.86	<u>50.80</u> / 86.54	80.57 / 71.48	<u>64.13</u> / <u>79.96</u>
AdaSCALE-L	<u>61.57</u> / <u>81.11</u>	48.78 / <u>86.40</u>	<u>75.88</u> / 73.02	62.08 / 80.18

Table 41. Near-OOD detection results (FPR@95 \downarrow / AUROC \uparrow) on ImageNet-1k benchmark using DenseNet-201 network. The best results are **bold**, and the second-best results are underlined.

Method	SSB-Hard	NINCO	ImageNet-O	Average
MSP	74.43 / 72.23	56.69 / 80.85	89.18 / 48.80	73.44 / 67.29
MLS	76.62 / 72.48	60.14 / 80.91	89.78 / 53.34	75.51 / 68.91
EBO	76.92 / 72.00	60.88 / 80.01	89.75 / 54.03	75.85 / 68.68
ReAct	78.62 / 70.93	57.51 / 81.19	73.78 / 68.83	69.97 / 73.65
ASH	78.80 / 68.71	63.84 / 79.45	80.07 / 68.19	74.24 / 72.12
SCALE	73.64 / 74.43	56.90 / 83.80	84.14 / 62.92	71.56 / 73.72
BFAct	81.57 / 67.52	65.10 / 77.38	66.93 / 72.93	71.20 / 72.61
LTS	73.46 / 74.36	57.54 / 83.79	82.87 / 65.52	71.29 / 74.56
OptFS	82.76 / 65.38	63.26 / 78.12	69.21 / 72.79	71.74 / 72.10
AdaSCALE-A	68.46 / 77.10	56.66 / 84.32	58.72 / 77.55	61.28 / 79.66
AdaSCALE-L	<u>68.97 / 76.85</u>	<u>57.96 / 83.92</u>	58.30 / 79.41	<u>61.75 / 80.06</u>

Table 42. Near-OOD detection results (FPR@95 \downarrow / AUROC \uparrow) on ImageNet-1k benchmark using EfficientNetV2-L network. The best results are **bold**, and the second-best results are underlined.

Method	SSB-Hard	NINCO	ImageNet-O	Average
MSP	81.28 / 75.03	57.97 / 86.70	78.26 / 80.53	72.51 / 80.76
MLS	84.74 / 73.50	72.88 / 84.83	86.71 / 79.32	81.44 / 79.22
EBO	85.27 / 71.58	75.81 / 82.07	87.49 / 77.81	82.86 / 77.15
ReAct	74.29 / 70.63	71.93 / 70.92	70.86 / 72.63	72.36 / 71.39
ASH	94.82 / 46.73	96.44 / 37.79	93.30 / 49.81	94.85 / 44.78
SCALE	90.16 / 57.07	89.93 / 59.69	89.03 / 63.60	89.70 / 60.12
BFAct	75.36 / 63.66	77.03 / 59.56	74.19 / 64.18	75.53 / 62.46
LTS	88.43 / 68.29	86.68 / 75.87	86.78 / 76.73	87.30 / 73.63
OptFS	74.68 / 73.83	70.24 / 76.18	71.94 / 75.86	72.29 / 75.29
AdaSCALE-A	<u>60.84 / 83.48</u>	47.45 / 89.47	<u>53.04 / 87.87</u>	53.78 / 86.94
AdaSCALE-L	53.56 / 85.00	<u>58.55 / 84.75</u>	52.72 / 87.58	<u>54.95 / 85.77</u>

Table 43. Near-OOD detection results (FPR@95 \downarrow / AUROC \uparrow) on ImageNet-1k benchmark using ViT-B-16 network. The best results are **bold**, and the second-best results are underlined.

Method	SSB-Hard	NINCO	ImageNet-O	Average
MSP	86.41 / 68.94	77.28 / 78.11	96.48 / 58.81	86.72 / 68.62
MLS	91.52 / 64.20	92.98 / 72.40	96.84 / 54.33	93.78 / 63.64
EBO	92.24 / 58.80	94.14 / 66.02	96.74 / 52.74	94.37 / 59.19
ReAct	90.46 / 63.10	78.50 / 75.43	90.94 / 66.53	86.63 / 68.35
ASH	93.50 / 53.90	95.37 / 52.51	94.47 / 53.19	94.45 / 53.20
SCALE	92.37 / 56.55	94.62 / 61.52	96.44 / 50.47	94.48 / 56.18
BFAct	89.81 / 64.16	71.37 / 78.06	85.09 / 69.75	82.09 / 70.66
LTS	91.42 / 64.35	82.63 / 75.48	92.42 / 62.46	88.83 / 67.43
OptFS	87.98 / 66.30	64.24 / <u>80.46</u>	77.43 / 71.43	76.55 / 72.73
AdaSCALE-A	<u>85.89</u> / 66.57	<u>61.92</u> / 80.47	67.81 / <u>72.37</u>	71.87 / <u>73.14</u>
AdaSCALE-L	<u>86.19</u> / 66.25	61.79 / 80.42	<u>67.99</u> / 73.01	<u>71.99</u> / 73.23

Table 44. Near-OOD detection results (FPR@95 \downarrow / AUROC \uparrow) on ImageNet-1k benchmark using Swin-B network. The best results are **bold**, and the second-best results are underlined.

Method	SSB-Hard	NINCO	ImageNet-O	Average
MSP	86.47 / 71.30	77.95 / 78.50	96.90 / 59.65	87.11 / 69.82
MLS	94.05 / 65.04	93.38 / 71.75	96.97 / 57.26	94.80 / 64.68
EBO	94.66 / 58.96	94.59 / 64.02	96.75 / 56.40	95.34 / 59.79
ReAct	89.19 / 68.70	68.54 / 80.16	90.20 / 70.93	82.64 / 73.26
ASH	97.15 / 45.47	96.64 / 47.36	95.32 / 49.92	96.37 / 47.58
SCALE	90.84 / 56.53	87.86 / 62.49	87.16 / 65.38	88.62 / 61.47
BFAct	84.86 / 69.41	61.30 / 81.10	69.27 / 75.34	71.81 / 75.28
LTS	90.36 / 64.51	81.02 / 74.23	88.44 / 62.92	86.61 / 67.22
OptFS	88.68 / 68.43	66.36 / 80.27	75.38 / <u>73.49</u>	76.81 / 74.06
AdaSCALE-A	80.10 / 70.46	64.67 / 81.10	75.46 / 71.87	73.41 / 74.48
AdaSCALE-L	<u>80.12</u> / <u>70.06</u>	63.68 / 81.35	<u>74.87</u> / 72.34	<u>72.89</u> / <u>74.58</u>

J.2. far-OOD detection

Table 45. Far-OOD detection results (FPR@95 \downarrow / AUROC \uparrow) on ImageNet-1k benchmark using ResNet-50 network. The best results are **bold**, and the second-best results are underlined.

Method	iNaturalist	Textures	OpenImage-O	Places	Average
MSP	43.34 / 88.41	60.87 / 82.43	50.13 / 84.86	58.26 / 80.55	53.15 / 84.06
MLS	30.61 / 91.17	46.17 / 88.39	37.88 / 89.17	55.62 / 84.05	42.57 / 88.19
EBO	31.30 / 90.63	45.77 / 88.70	38.09 / 89.06	55.73 / 83.97	42.72 / 88.09
ReAct	16.72 / 96.34	29.64 / 92.79	32.58 / 91.87	41.62 / 90.93	30.14 / 92.98
ASH	14.09 / 97.06	15.30 / 96.90	29.19 / 93.26	40.16 / 90.48	24.69 / 94.43
SCALE	9.50 / 98.02	11.90 / 97.63	28.18 / 93.95	36.18 / 91.96	21.44 / 95.39
BFAct	15.94 / 96.47	28.43 / 92.87	32.66 / 91.90	40.83 / 90.79	29.46 / 93.01
LTS	10.24 / 97.87	13.06 / 97.42	27.81 / 94.01	37.68 / 91.65	22.20 / 95.24
OptFS	15.88 / 96.65	16.60 / 96.10	29.94 / 92.53	40.24 / 90.20	25.66 / 93.87
AdaSCALE-A	7.61 / 98.31	<u>10.57 / 97.88</u>	<u>20.67 / 95.62</u>	32.60 / 92.74	17.86 / 96.14
AdaSCALE-L	<u>7.78 / 98.29</u>	10.33 / 97.92	20.61 / 95.62	<u>32.97 / 92.63</u>	<u>17.92 / 96.12</u>

Table 46. Far-OOD detection results (FPR@95 \downarrow / AUROC \uparrow) on ImageNet-1k benchmark using ResNet-101 network. The best results are **bold**, and the second-best results are underlined.

Method	iNaturalist	Textures	OpenImage-O	Places	Average
MSP	48.30 / 86.27	59.00 / 83.60	49.36 / 84.82	58.84 / 80.56	53.87 / 83.81
MLS	41.11 / 88.83	43.59 / 89.85	38.13 / 89.25	52.74 / 85.28	43.89 / 88.30
EBO	41.65 / 88.30	43.66 / 90.14	38.48 / 89.12	53.42 / 85.37	44.30 / 88.23
ReAct	19.86 / 95.66	26.94 / 93.78	30.18 / 92.54	42.58 / 90.41	29.89 / 93.10
ASH	19.90 / 95.68	13.94 / 97.32	27.76 / 93.63	43.11 / 89.59	26.18 / 94.06
SCALE	13.90 / 97.05	<u>9.34 / 98.04</u>	25.91 / 94.47	40.99 / 90.64	22.54 / 95.05
BFAct	19.60 / 95.69	25.79 / 93.79	30.18 / 92.55	42.14 / 90.13	29.43 / 93.04
LTS	15.07 / 96.83	10.33 / 97.89	25.51 / 94.52	41.40 / 90.53	23.07 / 94.94
OptFS	19.11 / 95.70	16.53 / 96.35	28.76 / 92.94	43.47 / 89.22	26.97 / 93.55
AdaSCALE-A	10.74 / 97.64	8.90 / 98.21	<u>18.75 / 96.03</u>	35.66 / 91.92	18.51 / 95.95
AdaSCALE-L	<u>11.71 / 97.36</u>	10.44 / 97.93	17.87 / 96.18	<u>36.57 / 91.55</u>	<u>19.15 / 95.76</u>

Table 47. Far-OOD detection results (FPR@95 \downarrow / AUROC \uparrow) on ImageNet-1k benchmark using RegNet-Y-16 network. The best results are **bold**, and the second-best results are underlined.

Method	iNaturalist	Textures	OpenImage-O	Places	Average
MSP	28.13 / 94.67	44.73 / 88.48	36.27 / 91.96	52.51 / 85.21	40.41 / 90.08
MLS	9.10 / 98.05	39.74 / 92.82	25.71 / 95.70	57.14 / 88.22	32.92 / 93.70
EBO	7.72 / 98.29	38.18 / 93.02	25.94 / 95.83	58.04 / 88.13	32.47 / 93.82
ReAct	21.24 / 94.14	41.20 / 87.25	43.46 / 89.20	74.92 / 74.10	45.20 / 86.17
ASH	48.89 / 87.39	45.75 / 88.79	70.98 / 82.52	72.99 / 77.06	59.65 / 83.94
SCALE	11.13 / 97.88	28.29 / 95.31	33.59 / 94.87	55.62 / 88.59	32.16 / 94.16
BFAct	37.88 / 86.24	54.87 / 77.64	62.53 / 79.59	79.46 / 65.39	58.69 / 77.22
LTS	14.29 / 97.52	<u>25.21</u> / <u>95.72</u>	43.38 / 93.53	57.08 / 87.51	34.99 / 93.57
OptFS	28.95 / 93.68	39.99 / 90.13	44.96 / 89.85	75.59 / 73.24	47.37 / 86.73
AdaSCALE-A	4.34 / 99.09	26.06 / 95.21	13.09 / 97.57	41.98 / 91.48	<u>21.37</u> / <u>95.84</u>
AdaSCALE-L	<u>4.41</u> / <u>99.02</u>	13.50 / 97.61	<u>18.56</u> / <u>96.92</u>	<u>43.93</u> / <u>91.22</u>	20.10 / 96.19

Table 48. Far-OOD detection results (FPR@95 \downarrow / AUROC \uparrow) on ImageNet-1k benchmark using ResNeXt-50 network. The best results are **bold**, and the second-best results are underlined.

Method	iNaturalist	Textures	OpenImage-O	Places	Average
MSP	43.56 / 88.04	62.23 / 82.13	48.06 / 85.65	58.42 / 81.02	53.07 / 84.21
MLS	32.96 / 90.93	51.58 / 87.39	37.33 / 89.80	57.76 / 83.77	44.91 / 87.97
EBO	33.42 / 90.54	51.73 / 87.56	37.79 / 89.72	57.56 / 83.62	45.12 / 87.86
ReAct	17.64 / 95.95	32.86 / 91.67	29.82 / 92.37	39.92 / 90.76	30.06 / 92.69
ASH	17.90 / 96.22	23.74 / 95.18	30.83 / 93.13	44.21 / 89.35	29.17 / 93.47
SCALE	15.66 / 96.75	27.75 / 94.94	31.43 / 93.41	47.62 / 89.08	30.62 / 93.54
BFAct	17.40 / 95.91	32.00 / 91.83	29.53 / 92.38	39.89 / 90.57	29.71 / 92.67
LTS	16.29 / 96.63	26.64 / 95.07	30.50 / 93.50	48.04 / 88.78	30.37 / 93.49
OptFS	17.20 / 96.12	23.11 / 94.69	29.59 / 92.75	40.24 / 90.05	27.54 / 93.40
AdaSCALE-A	10.02 / 97.80	17.99 / 96.38	<u>22.93</u> / <u>95.17</u>	37.38 / 91.62	22.08 / 95.24
AdaSCALE-L	<u>11.28</u> / <u>97.45</u>	<u>18.46</u> / <u>96.20</u>	21.23 / 95.35	<u>37.68</u> / <u>91.03</u>	<u>22.16</u> / <u>95.01</u>

Table 49. Far-OOD detection results (FPR@95 \downarrow / AUROC \uparrow) on ImageNet-1k benchmark using DenseNet-201 network. The best results are **bold**, and the second-best results are underlined.

Method	iNaturalist	Textures	OpenImage-O	Places	Average
MSP	42.02 / 89.84	62.33 / 81.56	50.31 / 85.19	59.74 / 81.14	53.60 / 84.43
MLS	31.99 / 92.11	57.75 / 85.56	42.70 / 88.28	61.30 / 83.82	48.43 / 87.44
EBO	33.12 / 91.46	57.47 / 85.55	43.75 / 87.91	61.46 / 83.67	48.95 / 87.15
ReAct	19.41 / 95.64	23.86 / 94.63	32.54 / 91.83	47.06 / <u>88.52</u>	30.72 / 92.65
ASH	21.57 / 95.47	21.42 / 95.56	41.23 / 90.19	49.80 / 87.45	33.50 / 92.17
SCALE	18.13 / 96.29	27.22 / 94.52	34.52 / 92.15	52.82 / 87.83	33.17 / 92.70
BFAct	20.64 / 95.42	21.70 / 95.17	39.76 / 89.97	<u>47.72</u> / 88.61	32.45 / 92.29
LTS	15.68 / 96.71	22.49 / 95.81	34.27 / 92.37	51.23 / 88.26	30.92 / 93.29
OptFS	25.81 / 93.92	21.75 / 95.01	38.45 / 89.67	51.66 / 85.54	34.42 / 91.04
AdaSCALE-A	17.30 / <u>96.03</u>	<u>19.42</u> / <u>96.23</u>	23.12 / <u>94.68</u>	52.20 / 85.98	<u>28.01</u> / 93.23
AdaSCALE-L	<u>17.97</u> / 95.87	16.87 / 96.69	<u>23.64</u> / 94.69	53.50 / 85.46	28.00 / <u>93.18</u>

Table 50. Far-OOD detection results (FPR@95 \downarrow / AUROC \uparrow) on ImageNet-1k benchmark using EfficientNetV2-L network. The best results are **bold**, and the second-best results are underlined.

Method	iNaturalist	Textures	OpenImage-O	Places	Average
MSP	<u>25.14</u> / 95.12	74.42 / 84.20	40.64 / 91.74	78.74 / 80.61	54.74 / 87.92
MLS	35.28 / 94.13	86.65 / 80.26	62.11 / 90.26	90.53 / 74.56	68.64 / 84.80
EBO	49.84 / 91.21	87.72 / 75.77	68.77 / 87.66	91.60 / 69.89	74.48 / 81.13
ReAct	46.44 / 80.96	54.56 / 77.17	60.79 / 78.20	78.39 / 64.99	60.05 / 75.33
ASH	96.26 / 37.76	95.40 / 50.98	97.52 / 43.19	97.07 / 34.34	96.56 / 41.57
SCALE	87.08 / 67.69	86.22 / 67.44	91.05 / 67.21	94.18 / 47.99	89.63 / 62.58
BFAct	57.31 / 69.11	63.43 / 67.70	69.30 / 67.49	76.86 / 58.52	66.72 / 65.70
LTS	79.05 / 84.72	86.89 / 75.39	88.00 / 81.53	93.45 / 63.56	86.85 / 76.30
OptFS	38.62 / 89.80	45.77 / 86.94	53.77 / 85.49	76.31 / 72.23	53.62 / 83.62
AdaSCALE-A	18.51 / 96.67	<u>42.07</u> / <u>90.56</u>	31.00 / 94.44	<u>58.87</u> / 84.26	37.61 / 91.48
AdaSCALE-L	26.58 / 95.02	32.81 / 92.38	39.19 / 92.31	56.66 / <u>82.33</u>	38.81 / 90.51

Table 51. Far-OOD detection results (FPR@95 \downarrow / AUROC \uparrow) on ImageNet-1k benchmark using Vit-B-16 network. The best results are **bold**, and the second-best results are underlined.

Method	iNaturalist	Textures	OpenImage-O	Places	Average
MSP	42.40 / 88.19	56.46 / 85.06	56.19 / 84.86	70.59 / 80.38	56.41 / 84.62
MLS	72.98 / 85.29	78.93 / 83.74	85.78 / 81.60	89.88 / 75.05	81.89 / 81.42
EBO	83.56 / 79.30	83.66 / 81.17	88.82 / 76.48	91.77 / 68.42	86.95 / 76.34
ReAct	48.22 / 86.11	55.87 / 86.66	57.68 / 84.29	75.48 / 77.52	59.31 / 83.65
ASH	97.02 / 50.62	98.50 / 48.53	94.79 / 55.51	93.60 / 53.97	95.98 / 52.16
SCALE	86.60 / 73.94	84.70 / 79.00	89.48 / 72.72	92.67 / 63.60	88.36 / 72.32
BFAct	40.56 / 87.96	48.65 / 88.31	48.24 / 86.59	68.86 / 80.21	51.58 / 85.77
LTS	50.42 / 88.92	61.70 / 86.53	69.26 / 83.45	76.07 / 78.82	64.37 / 84.43
OptFS	34.39 / 89.99	46.41 / 88.48	42.20 / 88.23	61.44 / 82.69	46.11 / 87.35
AdaSCALE-A	36.38 / 89.60	51.13 / 87.16	43.02 / 88.07	59.97 / 82.48	47.63 / 86.83
AdaSCALE-L	<u>35.16 / 89.84</u>	<u>50.91 / 87.37</u>	<u>43.01 / 88.13</u>	<u>60.05 / 82.55</u>	<u>47.28 / 86.97</u>

Table 52. Far-OOD detection results (FPR@95 \downarrow / AUROC \uparrow) on ImageNet-1k benchmark using Swin-B network. The best results are **bold**, and the second-best results are underlined.

Method	iNaturalist	Textures	OpenImage-O	Places	Average
MSP	55.63 / 86.47	79.28 / 80.12	81.22 / 81.72	77.41 / 79.78	73.39 / 82.02
MLS	93.46 / 78.87	94.60 / 74.73	97.61 / 70.72	94.97 / 69.17	95.16 / 73.37
EBO	95.11 / 67.72	95.36 / 69.69	97.97 / 60.19	95.87 / 58.35	96.08 / 63.99
ReAct	40.77 / 88.60	62.26 / 85.54	58.19 / 85.76	74.21 / 79.16	58.86 / 84.77
ASH	98.59 / 42.18	98.55 / 43.37	98.23 / 43.28	97.57 / 43.98	98.23 / 43.20
SCALE	87.83 / 62.98	87.71 / 69.63	88.75 / 66.63	82.08 / 67.82	86.59 / 66.77
BFAct	25.76 / 91.42	45.73 / 87.34	32.13 / 91.02	52.33 / 84.08	38.99 / 88.47
LTS	57.92 / 86.10	77.66 / 78.02	73.20 / 80.16	82.69 / 72.71	72.86 / 79.25
OptFS	31.94 / 90.56	<u>50.27 / 86.91</u>	<u>36.50 / 90.18</u>	58.38 / 83.51	44.27 / 87.79
AdaSCALE-A	32.82 / 90.73	61.82 / 85.34	38.58 / 89.78	58.02 / 82.71	47.81 / 87.14
AdaSCALE-L	<u>30.95 / 91.69</u>	60.17 / 86.30	37.52 / 90.08	<u>56.32 / 83.82</u>	46.24 / 87.97

J.3. Full-Spectrum near-OOD detection

Table 53. Near-FSOOD detection results (FPR@95 \downarrow / AUROC \uparrow) on ImageNet-1k benchmark using ResNet-50 network. The best results are **bold**, and the second-best results are underlined.

Method	SSB-Hard	NINCO	ImageNet-O	Average
MSP	88.17 / 47.34	78.15 / 54.73	96.29 / 13.81	87.54 / 38.63
MLS	90.04 / 43.32	82.06 / 50.23	95.59 / 18.94	89.23 / 37.50
EBO	90.19 / 42.62	82.64 / 49.01	95.54 / 19.57	89.46 / 37.07
ReAct	90.65 / 45.19	80.05 / 53.37	93.62 / 26.15	88.10 / 41.57
ASH	88.82 / 44.08	78.35 / 54.54	92.48 / 30.49	86.55 / 43.04
SCALE	85.85 / 48.10	77.54 / 57.01	93.26 / 32.58	85.55 / 45.90
BFAct	90.43 / 45.29	79.62 / 53.50	93.62 / 26.20	87.89 / 41.66
LTS	86.37 / 47.43	77.54 / 56.40	93.61 / 30.57	85.84 / 44.80
OptFS	90.78 / 44.01	77.24 / 54.91	90.91 / 32.26	86.31 / 43.73
AdaSCALE-A	81.30 / 51.88	74.13 / 58.55	89.15 / 37.62	81.52 / 49.35
AdaSCALE-L	<u>81.85 / 51.38</u>	<u>74.42 / 58.23</u>	<u>90.07 / 36.91</u>	<u>82.11 / 48.84</u>

Table 54. Near-FSOOD detection results (FPR@95 \downarrow / AUROC \uparrow) on ImageNet-1k benchmark using ResNet-101 network. The best results are **bold**, and the second-best results are underlined.

Method	SSB-Hard	NINCO	ImageNet-O	Average
MSP	87.09 / 49.18	76.45 / 56.92	94.24 / 28.33	85.93 / 44.81
MLS	88.90 / 46.45	79.19 / 53.62	93.94 / 31.76	87.34 / 43.94
EBO	89.02 / 45.99	79.60 / 52.66	93.87 / 32.40	87.50 / 43.68
ReAct	89.50 / 47.79	77.22 / 56.02	89.37 / 39.62	85.36 / 47.81
ASH	87.84 / 46.39	75.36 / 56.72	88.48 / 42.80	83.90 / 48.64
SCALE	85.81 / 48.94	75.33 / <u>58.79</u>	88.49 / 44.45	83.21 / 50.73
BFAct	89.19 / 48.07	76.94 / 56.02	89.54 / 39.65	85.22 / 47.91
LTS	86.02 / 48.72	<u>74.89</u> / 58.41	89.17 / 43.02	83.36 / 50.05
OptFS	89.63 / 46.23	75.52 / 56.71	85.82 / 44.21	83.65 / 49.05
AdaSCALE-A	82.33 / 51.47	74.38 / 59.17	<u>82.89 / 48.49</u>	79.87 / 53.04
AdaSCALE-L	<u>82.53 / 51.31</u>	75.22 / 58.62	82.19 / 48.03	<u>79.98 / 52.66</u>

Table 55. Near-FSOOD detection results (FPR@95 \downarrow / AUROC \uparrow) on ImageNet-1k benchmark using RegNet-Y-16 network. The best results are **bold**, and the second-best results are underlined.

Method	SSB-Hard	NINCO	ImageNet-O	Average
MSP	83.74 / 57.23	72.32 / 67.69	87.81 / 56.61	81.29 / 60.51
MLS	82.91 / 60.89	71.22 / 70.86	93.27 / 55.21	82.46 / 62.32
EBO	<u>82.77</u> / 61.63	<u>71.17</u> / <u>71.23</u>	93.39 / 55.02	82.44 / 62.63
ReAct	87.74 / 55.64	80.22 / 65.24	91.11 / 55.13	86.36 / 58.67
ASH	87.26 / 57.45	84.81 / 61.59	93.78 / 54.76	88.61 / 57.93
SCALE	83.23 / <u>61.02</u>	72.48 / 71.33	92.82 / 57.16	82.84 / 63.17
BFAct	90.46 / 54.73	87.03 / 61.98	92.37 / 54.13	89.96 / 56.95
LTS	83.53 / 60.77	74.23 / 70.84	92.30 / 57.71	83.35 / 63.11
OptFS	90.33 / 51.78	80.82 / 63.86	88.86 / 59.45	86.67 / 58.36
AdaSCALE-A	81.68 / 60.46	68.05 / 70.95	<u>83.25</u> / <u>60.91</u>	77.66 / 64.11
AdaSCALE-L	84.30 / 59.42	76.30 / 68.49	81.86 / 63.12	<u>80.82</u> / <u>63.68</u>

Table 56. Near-FSOOD detection results (FPR@95 \downarrow / AUROC \uparrow) on ImageNet-1k benchmark using ResNeXt-50 network. The best results are **bold**, and the second-best results are underlined.

Method	SSB-Hard	NINCO	ImageNet-O	Average
MSP	86.95 / 49.77	78.27 / 57.25	94.79 / 28.95	86.67 / 45.32
MLS	88.56 / 47.94	81.58 / 54.31	94.26 / 32.40	88.13 / 44.88
EBO	88.68 / 47.69	81.67 / 53.51	94.21 / 32.99	88.19 / 44.73
ReAct	89.45 / 47.44	80.37 / 55.29	91.40 / 37.58	87.07 / 46.77
ASH	86.26 / 49.73	79.62 / 57.17	92.63 / 39.67	86.17 / 48.86
SCALE	84.64 / 52.60	78.75 / <u>58.90</u>	94.20 / 37.99	85.86 / 49.83
BFAct	89.22 / 47.70	80.39 / 55.34	91.24 / 37.66	86.95 / 46.90
LTS	85.03 / 51.87	78.65 / 58.48	93.77 / 37.96	85.82 / 49.43
OptFS	89.63 / 46.23	<u>75.52</u> / 56.71	<u>85.82</u> / 44.21	83.65 / 49.05
AdaSCALE-A	82.33 / 51.47	74.38 / 59.17	82.89 / 48.49	79.87 / 53.04
AdaSCALE-L	<u>82.70</u> / <u>52.14</u>	75.85 / 58.05	89.55 / 43.81	<u>82.70</u> / <u>51.33</u>

Table 57. Near-FSOOD detection results (FPR@95 \downarrow / AUROC \uparrow) on ImageNet-1k benchmark using DenseNet-201 network. The best results are **bold**, and the second-best results are underlined.

Method	SSB-Hard	NINCO	ImageNet-O	Average
MSP	87.27 / 49.71	76.81 / 58.30	95.00 / 29.36	86.36 / 45.79
MLS	89.24 / 47.21	80.48 / 55.21	95.61 / 30.74	88.44 / 44.39
EBO	89.39 / 46.79	80.94 / 54.13	95.60 / 31.44	88.65 / 44.12
ReAct	90.76 / 45.54	79.54 / 55.57	88.40 / 42.63	86.23 / 47.91
ASH	89.75 / 47.08	81.35 / 58.13	90.47 / 46.81	87.19 / 50.67
SCALE	87.55 / 49.53	78.35 / 59.54	92.79 / 39.22	86.23 / 49.43
BFAct	92.33 / 44.88	83.90 / 54.83	84.88 / 49.50	87.04 / 49.74
LTS	87.30 / 50.02	<u>78.41</u> / 60.35	92.12 / 42.25	85.94 / <u>50.88</u>
OptFS	92.32 / 43.61	81.45 / 56.09	85.02 / 50.48	86.26 / 50.06
AdaSCALE-A	86.22 / 48.41	80.25 / 56.38	<u>81.35</u> / 47.45	82.60 / 50.75
AdaSCALE-L	<u>86.43</u> / <u>48.54</u>	80.83 / 56.30	81.00 / <u>50.00</u>	<u>82.75</u> / 51.61

Table 58. Near-FSOOD detection results (FPR@95 \downarrow / AUROC \uparrow) on ImageNet-1k benchmark using EfficientNetV2-L network. The best results are **bold**, and the second-best results are underlined.

Method	SSB-Hard	NINCO	ImageNet-O	Average
MSP	83.74 / 57.23	72.32 / 67.69	87.81 / 56.61	81.29 / 60.51
MLS	82.91 / 60.89	71.22 / 70.86	93.27 / 55.21	82.46 / 62.32
EBO	82.77 / 61.63	71.17 / 71.23	93.39 / 55.02	82.44 / 62.63
ReAct	87.74 / 55.64	80.22 / 65.24	91.11 / 55.13	86.36 / 58.67
ASH	87.26 / 57.45	84.81 / 61.59	93.78 / 54.76	88.61 / 57.93
SCALE	<u>83.23</u> / <u>61.02</u>	72.48 / 71.33	92.82 / 57.16	82.84 / 63.17
BFAct	90.46 / 54.73	87.03 / 61.98	92.37 / 54.13	89.96 / 56.95
LTS	83.53 / 60.77	<u>74.23</u> / <u>70.84</u>	92.30 / 57.71	83.35 / 63.11
OptFS	90.33 / 51.78	80.82 / 63.86	88.86 / 59.45	86.67 / 58.36
AdaSCALE-A	81.68 / 60.46	68.05 / 70.95	<u>83.25</u> / <u>60.91</u>	77.66 / 64.11
AdaSCALE-L	84.30 / 59.42	76.30 / 68.49	81.86 / 63.12	<u>80.82</u> / <u>63.68</u>

Table 59. Near-FSOOD detection results (FPR@95 \downarrow / AUROC \uparrow) on ImageNet-1k benchmark using Vit-B-16 network. The best results are **bold**, and the second-best results are underlined.

Method	SSB-Hard	NINCO	ImageNet-O	Average
MSP	92.28 / <u>47.57</u>	87.44 / 56.23	98.02 / 39.33	92.58 / 47.71
MLS	94.11 / 44.88	95.17 / 52.44	98.00 / 37.77	95.76 / 45.03
EBO	94.47 / 42.06	95.86 / 48.45	97.89 / 38.03	96.07 / 42.85
ReAct	94.95 / 41.84	88.65 / 52.48	95.21 / 44.64	92.94 / 46.32
ASH	88.95 / 56.47	91.09 / 55.11	90.00 / 55.78	90.01 / 55.79
SCALE	94.52 / 41.21	96.30 / 45.78	97.76 / 37.09	96.19 / 41.36
BFAct	94.99 / 41.44	85.62 / 53.35	92.62 / 45.64	91.07 / 46.81
LTS	95.33 / 43.36	90.52 / 53.14	95.90 / 41.30	93.91 / 45.93
OptFS	94.19 / 43.01	81.66 / <u>55.60</u>	88.90 / <u>46.04</u>	88.25 / 48.22
AdaSCALE-A	93.30 / 42.49	81.00 / 54.72	84.12 / 45.71	86.14 / 47.64
AdaSCALE-L	93.52 / 41.83	80.94 / 54.16	84.26 / 45.82	<u>86.24</u> / 47.27

Table 60. Near-FSOOD detection results (FPR@95 \downarrow / AUROC \uparrow) on ImageNet-1k benchmark using Swin-B network. The best results are **bold**, and the second-best results are underlined.

Method	SSB-Hard	NINCO	ImageNet-O	Average
MSP	91.55 / 53.29	86.73 / 60.62	97.85 / 42.90	92.04 / 52.27
MLS	94.49 / 50.01	93.94 / 56.40	97.11 / 43.76	95.18 / 50.06
EBO	94.66 / 47.41	94.58 / 52.04	96.76 / 45.84	95.33 / 48.43
ReAct	94.04 / 47.83	82.85 / 58.52	94.60 / 50.41	90.50 / 52.25
ASH	91.77 / <u>50.35</u>	90.91 / 52.09	88.80 / <u>54.50</u>	90.49 / 52.31
SCALE	93.39 / 47.38	91.25 / 53.00	90.80 / 56.10	91.81 / 52.16
BFAct	92.65 / 48.33	79.61 / <u>59.66</u>	84.26 / 53.17	85.51 / 53.72
LTS	94.26 / 48.70	88.32 / 57.60	93.04 / 46.33	91.87 / 50.88
OptFS	94.06 / 47.77	81.91 / 59.14	<u>86.95</u> / 51.34	87.64 / <u>52.75</u>
AdaSCALE-A	<u>90.29</u> / 46.84	81.54 / 57.44	87.74 / 47.55	86.52 / 50.61
AdaSCALE-L	90.18 / 46.63	<u>80.77</u> / 57.85	87.27 / 47.90	<u>86.07</u> / 50.79

J.4. Full-Spectrum far-OOD detection

Table 61. Far-FSOOD detection results (FPR@95 \downarrow / AUROC \uparrow) on ImageNet-1k benchmark using ResNet-50 network. The best results are **bold**, and the second-best results are underlined.

Method	iNaturalist	Textures	OpenImage-O	Places	Average
MSP	69.31 / 65.65	80.57 / 59.22	73.94 / 60.74	79.02 / 56.04	75.71 / 60.41
MLS	64.71 / 63.30	74.69 / 61.67	69.73 / 60.60	80.04 / 55.08	72.29 / 60.16
EBO	65.30 / 61.43	74.48 / 61.87	69.92 / 59.93	80.12 / 54.48	72.45 / 59.42
ReAct	51.90 / 75.79	63.55 / 69.22	65.64 / 67.36	71.81 / 67.01	63.22 / 69.84
ASH	49.21 / 76.93	50.54 / 77.64	63.04 / 69.03	70.62 / 64.79	58.35 / 72.10
SCALE	43.34 / 79.23	46.60 / 79.58	62.26 / 70.54	67.94 / 67.05	55.04 / 74.10
BFAct	51.01 / 75.85	62.45 / 69.03	65.52 / 67.21	71.17 / 66.45	62.54 / 69.63
LTS	45.12 / 78.72	48.77 / 79.13	62.43 / 70.17	69.31 / 66.20	56.41 / 73.55
OptFS	49.39 / 77.14	50.25 / 75.59	62.46 / 68.87	69.84 / 65.65	57.99 / 71.81
AdaSCALE-A	41.24 / 79.53	<u>45.55 / 79.64</u>	56.43 / 72.85	66.13 / 67.54	52.33 / 74.89
AdaSCALE-L	<u>41.75 / 79.63</u>	45.67 / 79.96	<u>56.80 / 72.82</u>	<u>66.69 / 67.28</u>	<u>52.73 / 74.92</u>

Table 62. Far-FSOOD detection results (FPR@95 \downarrow / AUROC \uparrow) on ImageNet-1k benchmark using ResNet-101 network. The best results are **bold**, and the second-best results are underlined.

Method	iNaturalist	Textures	OpenImage-O	Places	Average
MSP	71.78 / 64.51	78.82 / 62.20	72.52 / 62.27	78.71 / 57.55	75.46 / 61.63
MLS	70.55 / 62.07	72.11 / 65.46	68.68 / 62.27	77.60 / 58.03	72.23 / 61.96
EBO	70.94 / 60.64	72.18 / 65.71	68.96 / 61.59	77.97 / 57.75	72.51 / 61.42
ReAct	53.59 / 75.05	59.92 / 72.13	62.45 / 69.16	71.14 / 66.87	61.78 / 70.80
ASH	53.84 / 74.07	47.67 / 79.09	60.66 / 70.12	71.45 / 64.40	58.40 / 71.92
SCALE	47.82 / 76.79	42.04 / 80.95	59.26 / 71.76	70.32 / 65.86	54.86 / 73.84
BFAct	53.23 / 74.86	58.84 / 71.86	62.33 / 68.97	70.67 / 66.17	61.27 / 70.47
LTS	49.64 / 76.17	43.87 / 80.60	59.32 / 71.46	70.85 / 65.35	55.92 / 73.39
OptFS	51.52 / 75.52	48.88 / 76.96	59.99 / 70.28	70.86 / 65.15	57.81 / 71.98
AdaSCALE-A	44.77 / 77.51	42.17 / 80.73	<u>53.58 / 73.90</u>	67.14 / 66.84	51.91 / 74.75
AdaSCALE-L	<u>46.52 / 76.39</u>	<u>44.87 / 79.90</u>	53.32 / 73.81	<u>68.16 / 65.88</u>	<u>53.22 / 73.99</u>

Table 63. Far-FSOOD detection results (FPR@95 \downarrow / AUROC \uparrow) on ImageNet-1k benchmark using RegNet-Y-16 network. The best results are **bold**, and the second-best results are underlined.

Method	iNaturalist	Textures	OpenImage-O	Places	Average
MSP	53.98 / 80.49	69.36 / 70.97	62.02 / 75.95	75.48 / 65.76	65.21 / 73.29
MLS	39.99 / 85.09	69.12 / 73.89	58.30 / 80.08	79.98 / 66.96	61.85 / 76.51
EBO	38.42 / 86.11	68.23 / 74.16	58.77 / 80.93	80.56 / 67.08	61.49 / 77.07
ReAct	43.95 / 85.15	66.24 / 73.34	68.23 / 77.80	88.79 / 57.47	66.80 / 73.44
ASH	61.03 / 79.08	58.16 / 80.78	80.03 / 74.57	81.60 / 67.74	70.21 / 75.54
SCALE	39.13 / 86.34	56.30 / 79.93	60.66 / 81.10	76.25 / 70.04	58.09 / 79.35
BFAct	52.17 / 82.68	71.55 / 70.74	78.37 / 74.00	90.50 / 56.09	73.15 / 70.88
LTS	38.98 / 86.90	50.10 / 82.26	65.29 / 81.17	75.41 / 70.91	57.44 / <u>80.31</u>
OptFS	52.61 / 82.40	<u>62.47</u> / <u>76.57</u>	66.68 / 76.79	88.01 / 56.14	67.44 / 72.98
AdaSCALE-A	<u>34.25</u> / <u>87.68</u>	63.81 / 76.12	50.37 / <u>82.13</u>	<u>74.81</u> / 68.37	<u>55.81</u> / 78.58
AdaSCALE-L	32.72 / 88.82	47.93 / 82.84	<u>53.84</u> / 83.09	73.90 / <u>70.37</u>	52.10 / 81.28

Table 64. Far-FSOOD detection results (FPR@95 \downarrow / AUROC \uparrow) on ImageNet-1k benchmark using ResNeXt-50 network. The best results are **bold**, and the second-best results are underlined.

Method	iNaturalist	Textures	OpenImage-O	Places	Average
MSP	68.90 / 66.67	80.91 / 60.21	71.91 / 63.25	78.58 / 57.84	75.07 / 62.00
MLS	64.59 / 65.49	76.51 / 62.51	67.70 / 63.96	79.89 / 56.90	72.17 / 62.21
EBO	64.95 / 64.23	76.59 / 62.61	68.00 / 63.52	79.80 / 56.39	72.34 / 61.69
ReAct	51.97 / 76.08	65.34 / 68.27	63.05 / 68.94	70.13 / 67.58	62.62 / 70.22
ASH	53.84 / 74.07	47.67 / 79.09	60.66 / 70.12	71.45 / 64.40	58.40 / 71.92
SCALE	49.27 / <u>76.82</u>	60.07 / 75.14	62.91 / 70.69	73.38 / 64.22	61.41 / 71.72
BFAct	53.23 / 74.86	58.84 / 71.86	62.33 / 68.97	70.67 / 66.17	61.27 / 70.47
LTS	49.64 / 76.17	48.77 / <u>79.13</u>	62.43 / 70.17	70.85 / 65.35	<u>56.41</u> / <u>73.55</u>
OptFS	51.52 / 75.77	50.25 / 75.59	62.46 / 68.87	69.84 / 65.65	57.99 / 71.81
AdaSCALE-A	43.82 / 78.47	45.55 / 79.64	56.43 / 72.85	66.13 / <u>67.54</u>	52.33 / 74.89
AdaSCALE-L	<u>46.23</u> / 76.67	54.29 / 75.80	<u>56.84</u> / 72.44	<u>69.13</u> / 64.99	56.62 / 72.47

Table 65. Far-FSOOD detection results (FPR@95 \downarrow / AUROC \uparrow) on ImageNet-1k benchmark using DenseNet-201 network. The best results are **bold**, and the second-best results are underlined.

Method	iNaturalist	Textures	OpenImage-O	Places	Average
MSP	68.90 / 66.67	80.91 / 60.21	71.91 / 63.25	78.58 / 57.84	75.07 / 62.00
MLS	64.59 / 65.49	76.51 / 62.51	67.70 / 63.96	79.89 / 56.90	72.17 / 62.21
EBO	64.95 / 64.23	76.59 / 62.61	68.00 / 63.52	79.80 / 56.39	72.34 / 61.69
ReAct	51.97 / 76.08	65.34 / 68.27	63.05 / 68.94	<u>70.13</u> / 67.58	62.62 / 70.22
ASH	53.84 / 74.07	47.67 / <u>79.09</u>	60.66 / 70.12	71.45 / 64.40	58.40 / 71.92
SCALE	49.27 / 76.82	60.07 / 75.14	62.91 / 70.69	73.38 / 64.22	61.41 / 71.72
BFAct	53.23 / 74.86	58.84 / 71.86	62.33 / 68.97	70.67 / <u>66.17</u>	61.27 / 70.47
LTS	<u>49.64</u> / <u>76.17</u>	<u>48.77</u> / 79.13	62.43 / 70.17	70.85 / 65.35	56.41 / 73.55
OptFS	51.52 / 75.77	50.25 / 75.59	62.46 / 68.87	69.84 / 65.65	<u>57.99</u> / <u>71.81</u>
AdaSCALE-A	52.55 / 73.62	54.70 / 76.19	58.11 / <u>71.31</u>	77.77 / 58.83	60.78 / 69.99
AdaSCALE-L	53.04 / 73.62	51.83 / 78.00	<u>58.30</u> / 71.92	78.40 / 58.47	60.39 / 70.50

Table 66. Far-FSOOD detection results (FPR@95 \downarrow / AUROC \uparrow) on ImageNet-1k benchmark using EfficientNetV2-L network. The best results are **bold**, and the second-best results are underlined.

Method	iNaturalist	Textures	OpenImage-O	Places	Average
MSP	53.98 / 80.49	69.36 / 70.97	62.02 / 75.95	75.48 / 65.76	65.21 / 73.29
MLS	39.99 / 85.09	69.12 / 73.89	58.30 / 80.08	79.98 / 66.96	61.85 / 76.51
EBO	38.42 / 86.11	68.23 / 74.16	58.77 / 80.93	80.56 / 67.08	61.49 / 77.07
ReAct	43.95 / 85.15	66.24 / 73.34	68.23 / 77.80	88.79 / 57.47	66.80 / 73.44
ASH	61.03 / 79.08	58.16 / 80.78	80.03 / 74.57	81.60 / 67.74	70.21 / 75.54
SCALE	39.13 / 86.34	56.30 / 79.93	60.66 / 81.10	76.25 / 70.04	58.09 / 79.35
BFAct	52.17 / 82.68	71.55 / 70.74	78.37 / 74.00	90.50 / 56.09	73.15 / 70.88
LTS	<u>38.98</u> / 86.90	<u>50.10</u> / <u>82.26</u>	65.29 / 81.17	<u>75.41</u> / 70.91	<u>57.44</u> / <u>80.31</u>
OptFS	52.61 / 82.40	62.47 / 76.57	66.68 / 76.79	88.01 / 56.14	67.44 / 72.98
AdaSCALE-A	40.76 / 88.62	63.95 / 77.69	53.96 / 84.71	77.17 / 69.22	58.96 / 80.06
AdaSCALE-L	43.28 / <u>87.91</u>	<u>50.23</u> / 83.05	<u>57.11</u> / 84.45	73.87 / <u>70.29</u>	56.12 / 81.43

Table 67. Far-FSOOD detection results (FPR@95 \downarrow / AUROC \uparrow) on ImageNet-1k benchmark using ViT-B-16 network. The best results are **bold**, and the second-best results are underlined.

Method	iNaturalist	Textures	OpenImage-O	Places	Average
MSP	66.12 / 67.29	75.49 / 64.02	75.32 / 63.46	83.84 / 58.77	75.19 / 63.39
MLS	82.34 / 64.58	85.83 / 63.52	90.12 / 61.11	92.95 / 55.08	87.81 / 61.07
EBO	87.94 / 59.51	88.03 / 62.20	91.84 / 57.54	94.14 / 50.68	90.49 / 57.48
ReAct	70.31 / 62.56	75.49 / 64.90	76.64 / 61.30	87.02 / 54.77	77.37 / 60.88
ASH	93.23 / 53.23	95.19 / 51.16	90.38 / 57.95	89.04 / 56.56	91.96 / 54.72
SCALE	90.13 / 55.74	88.71 / 61.09	92.30 / 55.21	94.75 / 47.62	91.47 / 54.92
BFAct	66.39 / 62.89	71.84 / <u>65.55</u>	<u>71.56</u> / 62.19	84.23 / 55.84	73.51 / 61.62
LTS	71.01 / <u>67.15</u>	78.15 / 65.01	82.72 / 60.98	86.73 / 56.56	79.65 / 62.43
OptFS	62.89 / 66.41	70.96 / 65.68	68.25 / 64.30	80.02 / <u>58.53</u>	70.53 / 63.73
AdaSCALE-A	<u>65.49</u> / 65.27	74.75 / 63.69	<u>69.79</u> / 63.49	79.93 / 57.47	72.49 / 62.48
AdaSCALE-L	64.72 / 64.84	74.72 / 63.49	69.92 / 62.86	79.99 / 57.04	<u>72.34</u> / 62.06

Table 68. Far-FSOOD detection results (FPR@95 \downarrow / AUROC \uparrow) on ImageNet-1k benchmark using Swin-B network. The best results are **bold**, and the second-best results are underlined.

Method	iNaturalist	Textures	OpenImage-O	Places	Average
MSP	73.78 / 70.69	87.48 / 63.62	88.58 / 65.05	86.43 / 62.22	84.07 / 65.39
MLS	94.01 / 64.59	94.98 / 61.02	97.72 / 57.01	95.29 / 54.55	95.50 / 59.29
EBO	95.11 / 55.73	95.35 / 58.70	97.99 / 49.71	95.87 / 47.30	96.08 / 52.86
ReAct	66.17 / 68.53	79.27 / 66.85	76.92 / 65.82	85.99 / 57.89	77.09 / 64.77
ASH	94.55 / 47.18	94.43 / 48.22	93.77 / 48.28	92.55 / 48.99	93.82 / 48.17
SCALE	91.23 / 53.32	91.15 / 60.76	91.87 / 57.44	87.05 / 58.13	90.32 / 57.41
BFAct	54.53 / 73.59	69.73 / 68.65	59.76 / 74.29	74.09 / 64.30	64.53 / 70.21
LTS	72.97 / 70.44	86.21 / 62.18	83.29 / 63.87	89.39 / 56.32	82.96 / 63.20
OptFS	<u>58.91</u> / 71.84	72.14 / 68.00	62.45 / 72.16	77.16 / 63.35	67.66 / 68.83
AdaSCALE-A	61.33 / 68.58	79.90 / 64.03	65.40 / 67.52	77.68 / 59.21	71.08 / 64.83
AdaSCALE-L	60.15 / 70.58	78.72 / 65.23	64.83 / 68.17	<u>76.43</u> / 60.64	70.03 / 66.15

K. Visualizations of Score Separation

We present comparative visualizations of the energy score separation between SCALE and AdaSCALE using the RegNet-Y-16 architecture in terms of challenging near-OOD datasets below. As illustrated in Figure 6, AdaSCALE demonstrates a distinctively larger separation between ID and OOD score distributions compared to SCALE.

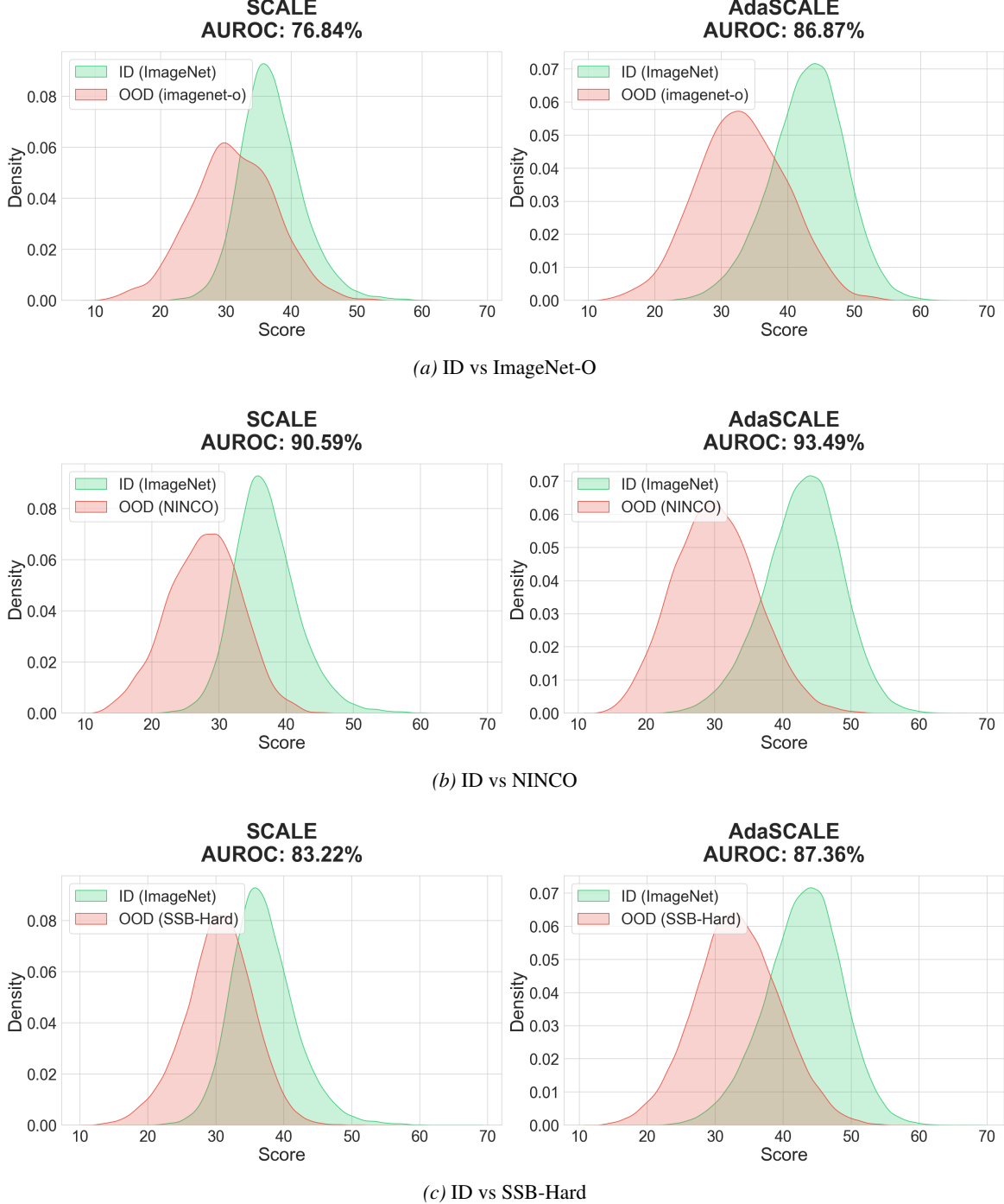


Figure 6. Comparative visualizations of score separation. AdaSCALE consistently shows reduced overlap between ID and OOD distributions compared to SCALE.